UNESCO Chair on Coastal Geo-Hazard Analysis
Research Institute for Earth Sciences
Geological Survey of Iran

Abstract:

The northward movement of the Arabian plate has resulted in forming the Zagros orogen as one of the most tectonically active intracontinental fold-thrust belts. The ongoing rapid convergence presents a remarkable seismic and aseismic crustal deformation across the Zagros. This thesis copes with the crustal deformation and active tectonics within the Zagros front employing a multidisciplinary approach integrating Interferometric Synthetic Aperture Radar (InSAR) as well as seismology, earthquake geology, tectonic geomorphology, field investigations, photogrammetry, quaternary geochronology, and seismic data interpretation. In order to obtain an accurate, quantitative measurement across the tectonically active Zagros front, stacks of SAR images have been employed to provide important constraints used to model the mechanisms of stress accumulation along the active faults.

ISBN: 978-622-5858-75-6

2024

UNESCO Chair on Coastal Geo-Hazard Analysis
Research Institute for Earth Sciences
Geological Survey of Iran

Active tectonics of the Zagros front

UCCGHA 019

2024

Active tectonics of the Zagros front

سرشناسه	:	فتحیان، آرام، ۱۳۶۲- -Fathian, Aram,1983
عنوان و نام پدیدآور	:	Active tectonics of the Zagros front[Book]/ author Aram Fathian bane; supervisors Klaus Reicherter...[et al.]; employer Faculty of Georesources and Materials Engineering of the RWTH Aachen University; with cooperation UNESCO Chair on Coastal Geo-Hazard Analysis.
مشخصات نشر	:	تهران: نشر خزه، ۱۴۰۲= ۲۰۲۴م.
مشخصات ظاهری	:	۱۳۰ ص.: مصور(رنگی)؛ ۱۴/۵ × ۲۱/۵ س‌م.
شابک	:	978-622-5858-75-6
وضعیت فهرست نویسی	:	فیپا
یادداشت	:	زبان: انگلیسی.
یادداشت	:	supervisors: Klaus Reicherter, Stefan Back, Stefano Salvi, Hamid Nazari
یادداشت	:	کتابنامه:ص. [۸۲]- ۱۳۰.
آوانویسی عنوان	:	اکتیوتکتونیک
موضوع	:	زمین‌شناسی ساختاری -- ایران -- البرز، زاگرس
موضوع	:	Structural Geology -- Iran -- Alborz -- Zagros
موضوع	:	گسله‌ها -- ایران -- کوه راگرس
موضوع	:	Faults -- Iran -- Zagros Mountains
شناسه افزوده	:	رایچرتر، کلاوس
شناسه افزوده	:	Reicherter, K. (Klaus)
شناسه افزوده	:	یونسکو. کرسی مخاطرات زمین شناختی ساحلی
شناسه افزوده	:	UNESCO Chair on Coastal Geo-Hazard Analysis
شناسه افزوده	:	دانشگاه فنی آخن. دانشکده مهندسی منابع زمین و مواد
شناسه افزوده	:	Rheinisch-Westfälische Technische Hochschule Aachen. Faculty of Georesources and Materials Engineering
رده بندی کنگره	:	الف۷ ۲۲۰۴۱ف/QE۶۰۱
رده بندی دیویی	:	۸/۵۵۱
شماره کتابشناسی ملی	:	۹۴۷۳۴۴۲

Active tectonics of the Zagros front

Author:

Aram Fathian

نشر خزه

نشر خزه

اطلاعات گزارش

عنوان: تکتونیک فعال جبهه زاگرس

مجری: دانشکده مهندسی منابع زمین و مواد دانشگاه RWTH آخن

زبان مرجع: انگلیسی

خروجی: گزارش، نقشه، مقاله، داده های الکترونیکی

ناظران علمی: کلاووس رایشرتر، استفان بَک، استفانو سالوی، حمید نظری

نویسنده: آرام فتحیان بانه

رئیس کرسی یونسکو در مخاطرات زمین شناختی ساحلی: حمید نظری

مسئول شورای اجرایی: راضیه لک

خلاصه‌نویسی: منوچهر قرشی

ناشر: نشر خزه

با همکاری کرسی یونسکو در مخاطرات زمین شناختی ساحلی

چاپ اول: ۱۴۰۲

شمارگان: ۵۰ نسخه

صفحات: ۱۳۰

شابک: ۶-۷۵-۵۸۵۸-۶۲۲-۹۷۸

khazepub@gmail.com

Report Information

Title: Active tectonics of the Zagros front

Employer: Faculty of Georesources and Materials Engineering of the RWTH Aachen University

Original language: English

Output: Report, Map, Paper, Digital Meta Data

Supervisors: Klaus Reicherter, Stefan Back, Stefano Salvi, Hamid Nazari

Author: Aram Fathian Beneh

Chairholder in the UNESCO Chair on Coastal Geo-Hazard Analysis: Hamid Nazari

Head of the Executive Council: Razyeh Lak

Summarized: Manouchehr Ghorashi

Publisher: Khazeh Publication

with cooperation UNESCO Chair on Coastal Geo-Hazard Analysis

First Edition: 2024

Edition number: 50

Page: 130

Shabak: 978-622-5858-75-6

khazepub@gmail.com

Scientific Council

Name	Affiliation
Ara Avagyan	IGS: Institute Geological Sciences
Rick J Bailey	IOC-UNESCO Indian Ocean Tsunami Warning and Mitigation System/ UNESCO
Aram Fathian Baneh	University of Calgary
Wenjiao Xiao	Chinese Academy of Sciences
Magdi Guirguis	Institut français d'archéologie orientale du Caire
Richard Walker	University of Oxford
Philippe Agard	University of Sorbonne
Justin Ahanhanzo	Intergovernmental Oceanographic Commission of UNESCO (IOC-UNESCO)
Alice Aurelie	UNESCO Water Sciences Division
Eric Barrier	University of Sorbonne
Jean-François Ritz	University of Montpellier
Martin Hanz	German under water archaeology association
Klaus Reicherter	Aachen University
Judith Thomalsky	German Archaeological Institute Tehran Branch
Hamid Alizadeh Lahijani	Iranian National Institute for Oceanography and Atmospheric Science
Abbas Banj Shafiei	Urmia University
Yahya Djamour	Shahid Beheshti University (SBU)
Hassan Fazeli Nashli	University of Tehran
Razyeh Lak	Research Institute for Earth Sciences
Mohammad Mokhtari	International Institute of Earthquake

	Engineering and Seismology
Hamid Nazari	Research Institute for Earth Sciences
Jafar Omrani	Geological Survey of Iran
Morteza Talebian	Research Institute for Earth Sciences
Mohammad Tatar	International Institute of Earthquake Engineering and Seismology
Mahdi Zare	International Institute of Earthquake Engineering and Seismology
Stefano Salvi	National Institute of Geophysics and Volcanology (INGV)
Ryo Anma	Tokushima University
Yeong Bae Seong	Korea University
John Lambert	Deltares, UNESCO
Issa El-Hussain	Sultan Qaboos University
Ekkehard Holzbecher	German University of Technology in Oman
Egor Krasinskiy	Underwater research center Russian Geographical Society
Audemard Franck A.	Department of Geology, Central University of Venezuela
Executive Committee	
Name	**Affiliation**
Nasir Ahmadi	Environmental Protection Organization of Mazandaran Province
Arash Amini	Golestan University
Alireza Amrikazemi	Scientific Coordinator, Qeshm Island UNESCO Global Geopark
Parviz Armani	Imam Khomeini International University
Ataollah Dadashpour	Geological Survey of Iran, Sari branch

Asghar Dolati	Kharazmi University
Hasan Fazelinashli	University of Tehran
Fahimeh Foroghi	Iranian National Institute for Oceanography and Atmospheric Science
Abdolazaim Ghanghormeh	Golestan University
Habibolah Ghasemi	Shahrood University of Technology
Mohammad reza Ghasemi	Research Institute for Earth Sciences
Manouchehr Ghorashi	Research Institute for Earth Sciences
Jafar Hassanpour	University of Tehran
Ataollah Kavian	Environmental Protection Organization of Mazandaran Province
Mohammadreza Kazemzadeh	Superme Audit Gourt
Razyeh Lak	Head of RIES and Executive Manager
Mahmoudreza Majidifard	Research Institute for Earth Sciences
Ali Akbar Momeni	Shahrood University of Technology
Babak Moradi	Iranian National Institute for Oceanography and Atmospheric Science
Seyed Mohsen Mortazavi	Hormozgan University
Hasan Nasrollah Zadeh Saravi	Caspian Sea Ecological Research Center
Ehsan Pegah	Kharazmi University
Abdolwahed Pehpouri	Qeshm Island UNESCO Global Geopark
Ahmadreza Rabani	University of Science and Technology of Mazandaran
Mahdi Rahmanian	Shargh Daily newspaper
Ahmad Rashidi	International Institute of Earthquake Engineering and Seismology
Masoud Sadri Nasab	University of Tehran
Mohammad Salamati	Respina Company

Mohammad Tatar	International Institute of Earthquake Engineering and Seismology
Alireza Vaezi	Research Institute for Earth Sciences
Mojtaba Yamani	University of Tehran
Ahmed Hadidi	German University of Technology in Oman (GUTECH)
Secretariat	
Name	**Affiliation**
Elnaz Aghaali	Research Institute for Earth Sciences
Keivan Ajdari	Research Institute for Earth Sciences
Hourieh AliBeygi	Research Institute for Earth Sciences
Sedigheh Ghanipour	Research Institute for Earth Sciences
Hamoon Memarian	Research Institute for Earth Sciences
Shirin Safavi	Research Institute for Earth Sciences
Aazam Takhtchin	Research Institute for Earth Sciences
Mehrnoosh Pour Saeid	Graphic Designer
Hanieh Bakhshaei	Geological Survey of Iran
Reza Behbahani	Geological Survey of Iran
Javad Darvishi khatooni	Geological Survey of Iran
Mohammadreza Ensani	Geological Survey of Iran
Marziyeh Estrabi Ashtiyani	Geological Survey of Iran
Gholamreza Hoseinyar	Geological Survey of Iran
Mojtaba Kavianpour Sangno	Geological Survey of Iran

Contents

Table of Figures

Figure 3: a) Regional tectonic setting of the Zagros orogen. White arrows and the numbers show the convergence velocity of the Arabian plate relative to the Eurasia fixed frame (Nocquet, 2012). Faults are compiled and modified after Berberian (1995), Berberian and Yeats (1999), Bahroudi and Talbot (2003), Hessami et al. (2003), Nazari et al. (2013), de Lamotte and Leturmy (2013), and Fathian et al. (2016). UDMA: Urmia-Dokhtar Magmatic Arc. b) Map of the Zagros orogeny structural subdivisions (see text for details). Orange circles highlight the earthquake epicenters from the Iranian Seismological Center online bulletin (IRSC; http://irsc.ut.ac.ir) for the period 2006 to 2018 highlighting the nucleation of the earthquakes on the slabs and edges of the tectonic salients and recessions (i.e., Kirkuk embayment, Lurestan Arc, Dezful embayment and Fars arc). Dark grey ellipses represent the meizoseismal area of the documented earthquakes (Ambraseys and Melville, 1982; Berberian and Yeats, 2001; Berberian, 2014). Red vectors show GPS velocities relative to the stable Eurasia frame (Khorrami et al., 2019). BF: Borazjan Fault; BRF: Bala Rud Fault system; DF: Dehshir Fault; HZF: High Zagros Fault; KF: Kazerun Fault; KhF: Khanaqin Fault; MFF: Main Front Fault; MRF: MISF: Masjid-i-Soleyman Fault; Main Recent Fault; MZRF: Main Zagros Reverse Fault; SF: Surmeh Fault; SPF: Sabz Pushan Fault; WF: Widyan Fault; ZFF: Zagros Foredeep Fault. c) Seismotectonic context of the study area. Orange circles show the earthquake epicenters from the IRSC online bulletin for

Melville, 1982; Berberian and Yeats, 1999, 2001; Berberian, 2014). Black, grey, blue, and red beachballs denote the earthquakes from the Global Centroid Moment Tensor (GCMT; https://www.globalcmt.org), body waveform (Maggi et al., 2000; Talebian and Jackson, 2004; Nissen et al., 2011), and first motion (Shirakova, 1967; McKenzie, 1972; Jackson and Fitch, 1981; Ni and Barazangi, 1986) catalogs, respectively. Red polygons highlight the outcropped diapirs. 63
Figure 10: Schematic 3D block diagram showing indenter tectonics in the Northwest Zagros controlled by lateral extrusion of the Lurestan Salient along the Khanaqin and Bala Rud transverse faults. Aseismic deformation uplifts the inner Lurestan Arc and the seismicity is concentrated on the front and the edges of the boundary between the Lurestan Arc and the Mesopotamian foreland basin (including the Kirkuk and Dezful Embayments). Two of the largest earthquakes documented in the Zagros (concentric black circles), the Saimareh (~9000 BCE; Mw 7.0) and Azgeleh (12 November 2017; Mw 7.3) events, are analogically located on the slab of Lurestan Salient lateral boundaries. Solid red line and dashed red line with triangles represent the surface projection of the modeled faults in this study. Black solid lines are the compiled and modified faults. Light and dark grey 3D arrows denote the horizontal, southwestward extrusion of the Lurestan salient, and vertical strain partitioning in the Lurestan Salient; brittle deformation concentrates in the front while the inner parts uplift mainly aseismically. Hatched

Table of Table

Abstract

The northward movement of the Arabian plate has resulted in forming the Zagros orogen as one of the most tectonically active intracontinental fold-thrust belts. The ongoing rapid convergence presents a remarkable seismic and aseismic crustal deformation across the Zagros. This thesis copes with the crustal deformation and active tectonics within the Zagros front employing a multidisciplinary approach integrating Interferometric Synthetic Aperture Radar (InSAR) as well as seismology, earthquake geology, tectonic geomorphology, field investigations, photogrammetry, quaternary geochronology, and seismic data interpretation.

In this thesis, in order to obtain an accurate, quantitative measurement across the tectonically active Zagros front, stacks of SAR images have been employed to provide important constraints used to model the mechanisms of stress accumulation along the active faults. I use the standard two-pass Differential SAR Interferometry (DInSAR) and Small Baseline Subset (SBAS) InSAR method (Berardino et al., 2002) to process a large number of SAR images to measure the coseismal and post seismic deformation due to the designated earthquakes-i.e., the Azgeleh, Tazehabad, and Sarpol-e Zahab (Chapter 3 and Chapter 6) earthquakes as

well as the Shonbeh (Chapter 5) and Fin earthquakes (Chapter 7).

Chapter 3 and Chapter 6 address the largest earthquake in the Zagros -the Azgeleh event- and the following seismic sequence with a hugely destructive impact on a widespread area on the Iran–Iraq border. With a strong focus on the application of the remotely sensed SAR data, I investigate three significant earthquakes and the relevant postseismic phase utilizing the constraints from our exclusive, temporary local seismic stations network. I quantify and introduce, for the first time, a complex fault setting involved in the seismic sequence. I additionally introduce the existence of unrecognized NE-SW trend and E-W trend for dextral and sinistral faulting within the Northwest Zagros. Providing the characteristics of the seismic sources, which is of high importance to the seismic hazard assessment, I also discuss the Coulomb stress changes within the region and emphasize some potential areas with a likelihood for future earthquake(s).

The Bushehr area (Chapter 4) provides a textbook example of fold-and-thrust belts, manifesting contemporaneous uplift, truncation, folding, faulting, and syn-kinematic offshore sedimentation. I provide detailed morphotectonic and Quaternary maps of the Bushehr area and document geomorphic markers associated with newly identified active faults and young

Quaternary folds in the area, such as the youngest and frontal-most active structures in the Zagros fold-and-thrust belt. Utilizing RTK GNSS/GPS surveys and Quaternary geochronology, I investigate and quantify the slip rates of the faults and the uplift rate within the Bushehr Peninsula. I interpret the offshore 2D seismic-reflection data and identify the subtle and young folding in the Persian Gulf. Integrating the onshore and offshore data, I evaluate and quantify the Quaternary and kinematic evolution of the truncated and uplifted structures in the Bushehr area, located in the lowland Zagros Foredeep.

I examine some of the reactivated, basement-involved Pan-African faults within the Zagros front. The Khanaqin fault (Chapter 3) and the Kazerun-Qatar lineament (Chapter 4) control the western boundaries of the Lurestan Arc and Fars Arc, respectively. This study presents a regional scale overview of the linkage between the identified active structures and the N-S orientation of these transverse faults outlining the indenter tectonics in the Zagros. The Darang fault (Chapter 5), identified in the Shonbeh seismic sequence, is another N-S-oriented strikeslip fault elongated east of the Kazerun-Qatar lineament.

I present a study on the Shonbeh earthquake of 9 April 2013 and the relevant seismic sequence (Chapter 5). I quantify the coseismic and postseismic deformation

fields and reconstruct the sources, validated by the relocation and fault plane solutions of the aftershocks, recorded by a local seismic stations network, which reveals a complex set of faulting involved in the seismic sequence. I also study the Fin doublet earthquake (Chapter 7) in the easternmost corner of the Zagros Simply Folded Belt (SFB). The InSAR and back-projection analyses reveal the characteristics of the mainshocks and the sub-events along a low-angle, south-dipping thrust zone within the eastern termination of the Zagros fold-and-thrust belt. The thesis synthesizes and concludes the data and results provided in this study on a regional scale, and describes the indenter and escape tectonics within the Zagros, showing a successful application and integration of the InSAR, seismology, and neotectonics to elaborate on the mapped and unmapped tectonically active structures (e.g., active faults) as well as to hypothesize the interaction of the identified sources with the present-day morphology within the deformation front of the Zagros orogen.

1 Scope

1.1 Motivation and societal relevance

The study of the seismic cycle deformation within a region is of high relevance in seismic hazard assessment. Historical and instrumental seismicity data

only constitute a minor part of the seismotectonic characteristics (including seismic potential) within a seismic region, to the extent that the existing catalogs are insufficient to cover the length of the earthquake cycle of the seismogenic faults, even in lands with ancient civilizations (e.g., Iran, China, and Italy), where earthquake events have long historical records.

Locating in the Alpine-Himalayan orogenic belt, Iranian territory is frequently menaced by strong earthquakes, this earthquake-prone plateau has experienced a vast number of historical and instrumental earthquakes that devastated many cities, and actually, some of the most populated cities of Iran, such as Tehran and Tabriz are in the vicinity of and/or adjacent to, or even crossed by seismogenic faults. The Rubar-Manjil area in northern Iran, the Bam and the Birjand areas in central and eastern Iran have experienced strong and deadly earthquakes during the last decades. Tehran, the capital, and the most populated city of Iran is surrounded by a set of seismogenic faults (e.g., the North Tehran, Mosha, and Taleghan faults). Tabriz, the highly populated city in NW Iran, is close to one of the most active faults in the Iranian plateau.

In fact, since 1900 A.D., several Iranian cities destroyed by great historical earthquakes have experienced weak instrumental seismicity (e.g., Ambraseys and Melville, 1982). This fact places these

cities in a critical condition since they have grown rapidly in terms of population, area, and economy in the last century, whereas seismic risk has not been strongly taken into consideration at the societal level. Drawing upon different approaches, plenty of researchers have studied the seismogenic behaviors of the active faults of Iran; nonetheless, little is known about their seismic cycle. Hence, it seems essential to apply cutting-edge, multi-disciplinary approaches in the identification of the characteristics of strain accumulation and release, in order to enhance our knowledge of the behavior of the seismogenic and tectonically active structures. This will actively contribute to developing the dataset necessary for the seismic hazard assessment within the seismically active regions in Iran.

2 Introduction

2.1 Study area

2.1.1 Regional setting

Iran is an active intra-continental collision zone (Figure 1) belonging to the Alpine-Himalaya orogenic belt (Jackson, 1992; Jackson and McKenzie, 1984). The belt contains convergence zones known as the African-

Eurasian, Indian-Eurasian, and Arabian-Eurasian zones, respectively. Iran belongs to the central portion of the belt, where its recent surface morphology is a result of the young (since Miocene) collision between Arabia (to the south) and Eurasia (to the north) plates (e.g., Agard et al., 2005). Within this portion of the belt, the deformation has been generally concentrated on two active zones—the Caucasus-TaleshAlborz (to the north) and the Zagros (to the south) zones (e.g., Berberian and King, 1981). The Red Sea Rifting causes a northward motion in the Arabian Plate against the Eurasian Plate situated in the northern region (e.g., Stöcklin, 1968; Falcon, 1974). Based on the GPS measurements, the convergence rate reaches 22–25 mm/yr (Nilforoushan et al., 2003; Vernant et al., 2004). Almost 50% of the total shortening that occurred within the Iranian territory is concentrated within the Zagros domain (e.g., Vernant et al., 2004; Mouthereau et al., 2012).

Seismicity in the Iranian plateau primarily focuses on the collisional areas that constitute the Makran to the south, the Zagros to the southwest, the Talesh, the central Alborz, and the Kopet Dagh to the north (e.g., Jackson and McKenzie, 1984). There is also a seismicity pattern along the major NNW-SSE strike-slip faults in central Iran (Figure 2). Based on historical seismic catalogs, over 450 destructive earthquakes have been recorded in Iran since 600 B.C. (Ambraseys and Melville, 1982; Berberian and Yeats, 1999, 2001;

Berberian, 2014). During the last century, strong earthquakes (M > 6.5) have occurred, with an average frequency of 5–8 years (Berberian, 2014; e.g., Salmas (1930; Ms = 7.4), Buin Zahra (1962; Ms = 7.2), Dasht-eBayaz (1968; Ms = 7.4), Tabas (1978; Ms = 7.7), Rudbar-Manjil (1990; Ms = 7.3), Furg (1990; Ms = 6.7), Qayen (1997; Ms = 7.3), Fandoqa (1998; Ms = 6.6), Bam (2003; Mw = 6.5), Khash (2013; Ms = 7.8), Azgeleh (2017; Mw = 7.3), and so on).

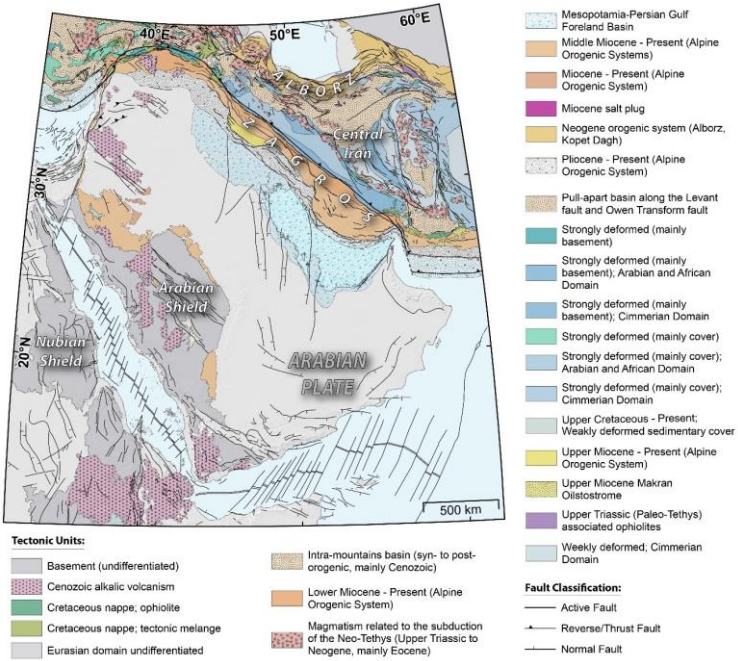

Figure 1: Tectonic context of the Arabia-Eurasia collisional zone. Faults are compiled and modified after Berberian (1995), Berberian and Yeats (1999), Hessami et al. (2003), Nazari et al. (2013), and Fathian et al. (2016). Tectonic units and Arabian plate faults are modified after de Lamotte and Leturmy (2013) and Fathian et al. (2021).

2.1.2 The Zagros Mountains

Extending from the Taurus Mountains (northeastern Turkey) to the Strait of Hormuz (southern Iran), the 1800-km long Zagros is one of the world's most active and youngest orogens. This range, with ca.

300 km in width, accommodates a high rate of deformation and seismic activity (Falcon, 1969; Haynes and McQuillan, 1974; Berberian, 1995; Hessami et al., 2001; Talebian and Jackson, 2004). The closure of the Neo-Tethyan Ocean due to the NE-dipping subduction of the Arabian plate below the Iranian micro-continent and a subsequent collision -beginning in the Neogene- has formed this fold-thrust belt (Stöcklin, 1968; Falcon, 1974; Berberian and King, 1981; Berberian et al., 1982; Berberian, 1983, 1995; Alavi, 1994).

The Zagros seismicity is delimited to a ca. 200 km wide zone of small- to mid-sized earthquakes between the Main Zagros Reverse Fault (MZRF) and the Persian Gulf (Figure 2). The earthquakes mainly occur along the oblique-slip faults (e.g., the MZRF and the Kazerun fault), the high-angle reverse faults that strike parallel to the trend of the fold axes, and/or the master blind thrust faults (Jackson and McKenzie, 1984; Baker et al., 1993; Ni and Barazangi, 1986; Berberian, 1995; Karasözen et al., 2019). Unlike in the other seismotectonic provinces of Iran (e.g., the Alborz and Central Iran), both large earthquakes and surface ruptures in the Zagros are rarely observed (Ambraseys and Melville, 1982; Talebian and Jackson, 2004; Berberian, 2014).

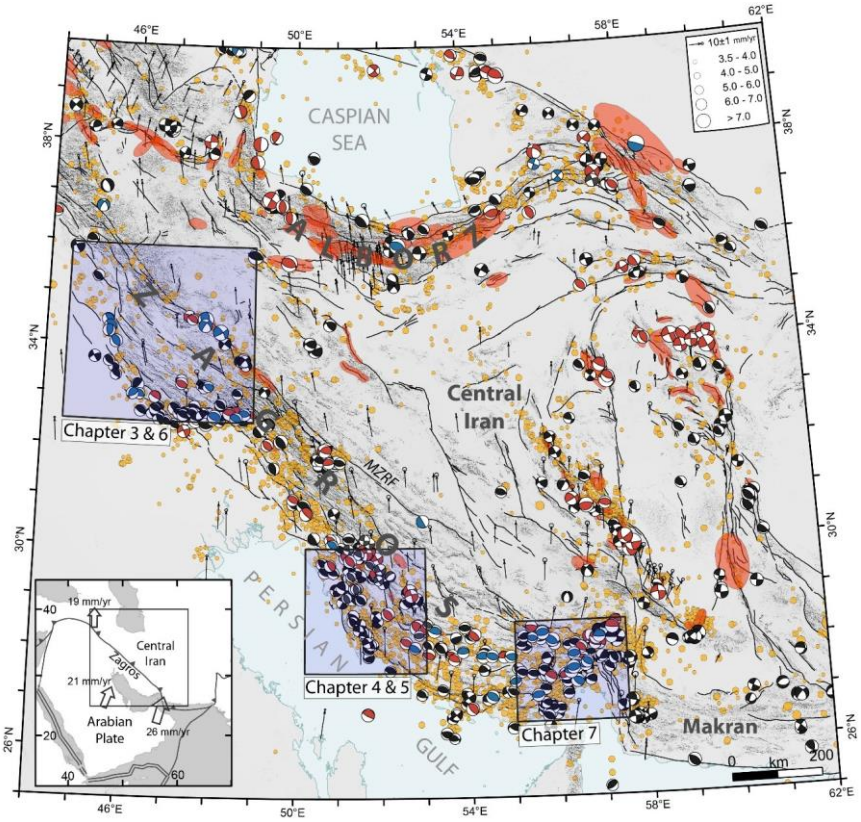
CASPIAN SEA
ALBORZ
ZAGROS
Central Iran
MZRF
PERSIAN GULF
Chapter 3 & 6
Chapter 4 & 5
Chapter 7
Makran
Central Iran
Zagros
Arabian Plate
19 mm/yr
21 mm/yr
26 mm/yr
10±1 mm/yr
3.5 - 4.0
4.0 - 5.0
5.0 - 6.0
6.0 - 7.0
> 7.0
0 km 200

Figure 2: Seismotectonic setting of Iran. Faults are compiled and modified after Berberian (1995), Berberian and Yeats (1999), Hessami et al. (2003), and Fathian et al. (2016, 2021). Red, blue, and black beachballs symbolize fault plane solutions from the body waveform (Maggi et al., 2000; Talebian and Jackson, 2004; Nissen et al., 2011), the first motions (Shirakova, 1967; McKenzie, 1972; Jackson and Fitch, 1981; Ni and Barazangi, 1986; Nissen et al., 2019), and the Global Centroid Moment Tensor (GCMT; https://www.globalcmt.org) catalogs. Compared to a large number of historical earthquakes (red ellipses; Ambraseys and Melville, 1982; Berberian, 1995; Berberian and Yeats, 1999, 2001) in northern Iran (e.g., the Alborz), the Zagros in the southwest reflects much fewer in number historical events but intense instrumental seismicity. Orange circles denote the epicenter of the earthquakes (IRSC; http://irsc.ut.ac.ir). The study areas and the corresponding chapters of the thesis are demonstrated by transparent blue rectangles.

The Zagros Fold-Thrust Belt (ZFTB) is the external subdomain of the Zagros orogen (e.g., Alavi, 2007) where approximately one-half to one-third of the present-day convergence rate (22 ± 2 mm/y) is represented by seismic deformation. In this thesis, I have focused on the very outer part of the ZFTB -the Zagros front-where significant seismic events have occurred close to the borders of the domain (Figure 2).

2.2 Methods and data

In this thesis, to complete the dataset necessary for seismic hazard assessment in Iran, I try to provide brand new data by focusing on active tectonics in the Zagros front utilizing a multidisciplinary approach. A wide range of methods, including Space-borne

Interferometric Synthetic Aperture Radar (InSAR) techniques, morphotectonics, seismology, paleoseismology, and remote sensing come together combined with data modeling and field surveys to accomplish the study. Since the methods are explained in detail in Chapters 3–7, in this section, I briefly elaborate on some of the methods applied in the thesis.

2.2.1 InSAR

Crustal deformation is one of the most important parameters used for the observation and modeling of the seismic cycle of strain accumulation and release. The improvements in satellite Earth Observation data and methods over the last two decades have provided a way to measure crustal movements with good accuracy and spatial coverage. In particular, multi-temporal Synthetic Aperture Radar (SAR) satellite data sets and SAR interferometric techniques have demonstrated the capacity to obtain information on the dynamics of the deformation occurring during an earthquake and then the following post-seismic phase. Table 1 lists the SAR dataset used in this thesis.

Synthetic Aperture Radar Interferometry (InSAR) can measure the projection of the deformation vector onto the Line of Sight (LOS) direction providing unique capabilities for the study of crustal deformation and active processes. In fact, InSAR is a remote-sensing

technique and does not require fieldwork, and can be available practically worldwide. SAR is a coherent active microwave image instrument, which can acquire data during daytime or nighttime, and virtually under all meteorological conditions. The phase difference between the two acquisitions can be related to the changes in the geometric distance of the radar antenna from the illuminated object, provided the backscattered signals are sufficiently correlated (Bürgmann et al., 2000; Massonnet et al., 1993; Zebker et al., 1994).

Several issues, however, may complicate the application of InSAR to a single image pair. Firstly, several sources (e.g., vegetation, ground movement, soil erosion, etc.) may cause the SAR phases at the two acquisitions to be statistically decorrelated (Zebker and Villasenor, 1992), and thus unrelated to the changes in the geometric distance from the radar. The recovery of the integer multiples of 2π, and hence the determination of the phase gradient between any two interferogram pixels, represents a 2D phase unwrapping problem, for which only approximate solutions can be found. Finally, the measured differences in travel times (or distances) can also be influenced by unmodeled effects, e.g., due to variable propagation velocity through the variably refractive atmosphere (mainly due to water vapor content in the troposphere and Total Electron Content in the ionosphere) and to uncertainties in the satellite position.

Nevertheless, the accuracy of the obtained measurements affecting the surface after an event is about 1–2 cm.

To overcome the aforementioned limitations relative to using a single differential SAR interferometry (DInSAR) pair, in the last 2 decades Multi-Temporal InSAR techniques (MTInSAR) were developed which exploit the redundancy offered by tens or hundreds of image pairs to reduce such issues (e.g., Bürgmann et al., 2000). The output of these techniques are the ground displacement time series and the mean velocity along the LOS, temporally referred to the first acquisition date of the analyzed image stack, and spatially referred to a reference point or area within the studied area of interest.

Table 1: Space-borne Synthetic Aperture Radar (SAR) images used to estimate the coseismic and postseismic phases of the selected earthquakes in this thesis. JAXA: The Japan Aerospace Exploration Agency; ESA: The European Space Agency; ASI: The Italian Space Agency; CSA: The Canadian Space Agency.

**The table is presented on the next page

Event	Phase	Satellite	Path	Orbit	Acquisition	Type	Scenes	Source
Azgeleh	Coseismic	ALOS-2	180	Ascending	WD	L-Band	2	JAXA
		ALOS-2	71	Descending	WD	L-Band	2	JAXA
		Sentinel-1	174	Ascending	IW	C-Band	2	ESA Copernicus
		Sentinel-1	6	Descending	IW	C-Band	2	ESA Copernicus
		Sentinel-1	72	Ascending	IW	C-Band	2	ESA Copernicus
		Sentinel-1	79	Descending	IW	C-Band	2	ESA Copernicus
	Postseismic	Sentinel-1	72	Ascending	IW	C-Band	32	ESA Copernicus
		Sentinel-1	79	Descending	IW	C-Band	31	ESA Copernicus
		COSMO-SkyMed	H4-0B	Descending	STRIPMAP	X-Band	36	ASI
		COSMO-SkyMed	H4-10	Ascending	STRIPMAP	X-Band	28	ASI
		COSMO-SkyMed	H4-0B	Ascending	STRIPMAP	X-Band	52	ASI
Tazehabad	Coseismic	Sentinel-1	72	Ascending	IW	C-Band	2	ESA Copernicus
		Sentinel-1	174	Ascending	IW	C-Band	2	ESA Copernicus
		Sentinel-1	6	Descending	IW	C-Band	2	ESA Copernicus
Sarpol-e Zahab	Coseismic	Sentinel-1	6	Descending	IW	C-Band	2	ESA Copernicus
		Sentinel-1	72	Ascending	IW	C-Band	4	ESA Copernicus
		Sentinel-1	6	Descending	IW	C-Band	2	ESA Copernicus
		Sentinel-1	79	Descending	IW	C-Band	2	ESA Copernicus
Shonbeh	Coseismic	RADARSAT-2	–	Descending	Wide 1	C-Band	2	CSA
	Postseismic	COSMO-SkyMed	H4-03	Descending	STRIPMAP	X-Band	21	ASI
		COSMO-SkyMed	H4-16	Ascending	STRIPMAP	X-Band	18	ASI
		COSMO-SkyMed	H4-05	Ascending	STRIPMAP	X-Band	51	ASI
Fin Doublet	Coseismic	ALOS-2	65	Descending	WD	L-Band	2	JAXA
		Sentinel-1	166	Descending	IW	C-Band	2	ESA Copernicus
		Sentinel-1	57	Ascending	IW	C-Band	4	ESA Copernicus

The existing MT-InSAR algorithms fall into two categories, namely the Persistent Scatterer (PS) (Ferretti et al., 2001) and the Small Baseline (SBAS) (Berardino et al., 2002) approaches, although more recently hybrid algorithms exploiting the basic principles of both methodologies have also been proposed (Hooper, 2008). The PS methods aim to identify coherent radar targets exhibiting a high phase stability over the whole temporal span of the observations. These targets are only slightly affected by temporal and geometrical decorrelation, and often correspond to man-made structures or bare rocks. In contrast, in the original SBAS approach (Berardino et al., 2002), interferometric pairs are chosen to minimize temporal and geometric decorrelation, allowing deformation time series to be retrieved for distributed scatterers, i.e., neighboring radar resolution cells, which are not dominated by a single scatterer and share the same backscattering properties. In the best case, both PS and SB multi-temporal InSAR approaches can reach accuracies as high as 1 mm/yr (Casu et al., 2006; Hooper et al., 2012).

The workflow for the SBAS module in the SARscape® software is: (i) connection graph generation (a network of image pairs); (ii) interferometric step, which generates a stack of interferograms, and filters them using the Goldstein adaptive filter (Goldstein and Werner, 1998), and then the phase is unwrapped using the Minimum Cost Flow (MCF) method (Costantini,

1998); (iii) refinement and re-flattening, which estimates and removes the topographic and constant phases as well as the possible phase ramps from the unwrapped stack; (iv) first inversion, the first estimate of the displacement rate and residual heights are calculated and used to re-flatten the interferograms. A second unwrapping is also performed; (v) the second inversion removes the atmospheric phase component to clean and calculate the final displacement velocity and time series; (vi) geocoding of the final products.

2.2.2 Seismology

To study the microseismicity of the seismic sequence following the main events of Azgeleh (Chapter 3) and Shonbeh (Chapter 5), local seismological networks were installed. The operated network, including CMG-6TD, 3-component seismometers, CMG-5TD accelerometers connected to CMG-DM24 Guralp recorders, and Titan digitizer connected to 20-s 3-component Lennartz seismometers, recorded the aftershocks for a 7- and 6-week period for the Azgeleh and Shonbeh seismic sequence, respectively. The aftershocks are initially processed based on the proposed velocity model for the Zagros (Hatzfeld et al., 2003). Constraining an azimuthal gap less than 180°, root mean square traveltime residual (RMS) less than 0.2 s as well as the epicenter and depth uncertainties of less than 2 km, a subset of the aftershock, recorded by at least 10

stations, is selected. The subsets are employed in the VELEST program (Kissling, 1988) to obtain appropriate velocity models based on 1D inversion *P* and *S* arrival times of bestlocated aftershocks, and located the selected events with the Hypocenter 3.2 program (Lienert and Havskov, 1995).

Back-projection analysis of seismic events (Chapter 7) is a technique that has been widely used to study shallow earthquakes (e.g., Ishii et al., 2005, 2007; K. T. Walker et al., 2005; Pulido et al., 2008; Walker and Shearer, 2009; Honda and Aoi, 2009). The back-projection method processes arrays of coherent waveforms and images the earthquakes by time reversing seismograms from an array to a grid of potential source locations (Kiser et al., 2011; Kiser and Ishii, 2017) based on a one-dimensional seismic model such as IASP91 (Kennett and Engdahl, 1991):

$$sj(t) = \sum_{i=1}^{N} \omega ij(t) fij(t + \tau ij)$$

where $s\ j(t)$ is a stacked time series, at a source grid point j, dependent on time (t). N is the total number of the seismic stations, and ωij is the weighting function for station i and source point j. τij is predicted time shift at the ith station to the jth grid point (e.g., Kiser and Ishii, 2017).

2.2.3 Neotectonics

Morphotectonic investigations within the study areas were made via a combination of approaches, to gather and produce data to infer the tectonically active structures and their kinematics.

Following the mapping based on the satellite imagery, field studies with both classical and neotectonic approaches were performed to prepare detailed Quaternary and morphotectonic maps (e.g., Chapter 4 and Chapter 5). In the Bushehr area, 25 test pits (approximately 1 m in depth, length, and width) were excavated to collect sediments as well as Optically Stimulated Luminescence (OSL) (e.g., Rhodes, 2011) and radiocarbon (^{14}C) (e.g., Walker, 2005) samples to classify the sediments and define the age of the sedimentary units. Two sites on the uplifted marine terraces and two selected sites along the newly introduced Khormuj fault zone and the relevant morphotectonic features were also investigated by RTK GNSS/GPS to generate highresolution digital surface models (DSM) of the sites. Paleoseismological investigations were also performed along the Khormuj fault with a surface signature. We additionally used 2D reflection seismic data to study the offshore area of Bushehr (Chapter 4). All seismic interpretations were executed through the Kingdom Suite software.

The field investigations corresponding with Chapter 3 are not reported in this thesis, and the field observations will be used in an independent study on the coseismic slope instabilities and superficial features due to the Azgeleh earthquake.

3 Complex co- and postseismic faulting of the 2017– 2018 seismic sequence in western Iran revealed by InSAR and seismic data

Abstract

The largest earthquake in the Zagros Mountains struck the city of Azgeleh on the Iran–Iraq border on 12 November 2017. This Mw 7.3 earthquake was followed by an intense seismic sequence. Implementing the double-difference earthquake location technique, we relocate 1069 events recorded by our local seismic network deployed after the mainshock. The spatial distribution of the epicenters indicates linear alignments of the events nucleated along at least four notable clusters. The clusters are characterized by at least one significant earthquake, such as the Tazehabad earthquake of 25 August 2018 (Mw 5.9) along a dense, east-west trending cluster and the Sarpol-e Zahab earthquake of 25 November 2018 (Mw 6.3) along the cluster with a

northeast-southwest trend. We use two-pass differential SAR interferometry (DInSAR) and Small BAseline Subset (SBAS) methods to study the coseismic permanent displacements of the Azgeleh, Tazehabad, and Sarpol-e Zahab events as well as the one-year postseismic deformation field of the 2017–2018 seismic sequence, respectively. We use non-linear and linear optimization algorithms to derive the source geometry and the slip distribution along the fault planes. The inversion is conducted by introducing also seismological constraints, leading to the definition of a listric geometry for the Azgeleh mainshock rupture that accommodates the slip area at depth of 10–16 km along a sub-horizontal plane (dipping ~3°) and a low-angle (~16°) ramp. The thrust and dextral movements along this NNW-striking (~345°) fault have triggered a tear fault responsible for the Tazehabad event ruptured an eastwest trending (~267°), north-dipping (~78°) sinistral shear fault. We present the dextral slip distribution of the Sarpol-e Zahab event along a NE-striking (~34°) fault, as a synthetic Riedel structure for the southern segment of the Khanaqin fault, dipping 63° to the southeast. We find the postseismic deformation field associated with the seismic sequence is not confined only to the mainshock source (the Azgeleh fault), but also develops along the Tazehabad and Sarpol-e Zahab faults. We additionally propose afterslip along a duplex, flat-ramp-flat structure downdip and up-dip of the Azgeleh coseismic slip area.

The up-dip afterslip develops onto the shallow detachment (~3°) at depth of ~8 km and the down-dip afterslip propagates onto the mid-crustal décollement level within the Pan-African basement. The Azgeleh, Tazehabad, Sarpol-e Zahab, and Khanaqin faults mark the Lurestan Arc-Kirkuk Embayment sharp margin in the Northwest Zagros and play a key role in the lateral escape of the Lurestan Salient and vertical strain partitioning in the Zagros front.

3.1 Introduction

Located in the central part of the Alpine-Himalayan orogenic belt, the Zagros orogen is one of the youngest and most tectonically active intra-continental belts in the world (e.g., Haynes and McQuillan, 1974; Stöcklin, 1974; Blanc et al., 2003). Due to the ongoing Iran-Arabia NS convergence (Figure 3a), the NW-SE-oriented Zagros Mountains are still under deformation by ~50% of the measured convergence rate (22 ± 2 mm/y) (e.g., Vernant et al., 2004). The Zagros Mountains (Figure 3b) consist of three main tectonostratigraphic domains including, from southwest to northeast, the Mesopotamia-Persian Gulf Foreland Basin, the Zagros FoldThrust Belt (ZFTB), and the Zagros Imbricated Zone (ZIZ; also known as High Zagros Zone: HZZ).

The ZFTB, as the external part of the Zagros Mountains, includes three subdomains: The Zagros

Foredeep Zone, the Mountains Front Flexure Zone (MFFZ), and the Simply Folded Belt (SFB) (Falcon, 1974; Berberian, 1995; Bahroudi and Koyi, 2003, 2004; Alavi, 2007). In the area, there are four physiographic provinces, namely the Kirkuk Embayment, the Lurestan Arc (also known as the Pusht-e Kuh Province), the Dezful Embayment, and the Fars Arc (Figure 3c) (Stöcklin, 1968; Bahroudi and Koyi, 2004; Alavi, 2007). The domains and subdomains of the Zagros are mainly separated by the master blind thrust faults (Figure 3b), such as the Zagros Foredeep Fault (ZFF), the Main Front Fault (MFF), the High Zagros Fault (HZF), the Main Recent Fault (MRF), and the Main Zagros Thrust Fault (MZT), as introduced by Berberian (1995). These basement-involved thrust faults cut through the folded Phanerozoic sedimentary cover and control the deformation of the cover in a thin-skinned tectonic regime (e.g., Berberian, 1995; Motagh et al., 2015; Copley et al., 2015). The Zagros accommodates intense, low- to moderate-magnitude seismic events (e.g., Barnhart et al., 2013; Karasözen et al., 2019). The earthquakes in the Zagros are distributed across a ~200 km wide zone (Figure 3b), commonly along the master blind thrust faults (e.g., Berberian, 1995), within the sedimentary cover-between 8 to 14 km-beneath the Hormuz Salt Formation (Jackson and Fitch, 1981; Ni and Barazangi, 1986; Baker et al., 1993; Hessami et al., 2001). The lower Cambrian Hormuz, consisting of salt

units in the Fars Arc and shales in the Lurestan Arc, detach the sedimentary cover from the crystalline basement (Berberian, 1995; McQuarrie, 2004; Sherkati and Letouzey, 2004; Alavi, 2007). Thus, due to the influence of the Hormuz units, surface faulting in the Zagros is observed in rare cases (e.g., Talebian and Jackson, 2004; R. T. Walker et al., 2005) and the surface is truncated and accommodates parallel folds (e.g., Nissen et al., 2011).

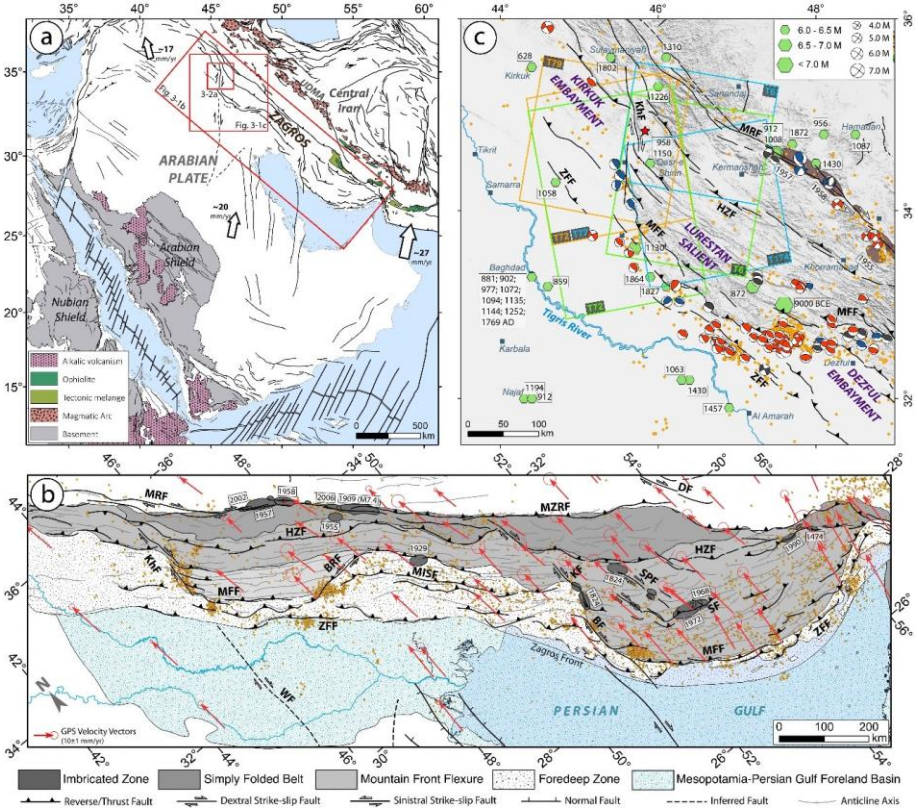
a
c
b
ARABIAN PLATE
Central Iran
ZAGROS
Arabian Shield
Nubian Shield
Alkalic volcanism
Ophiolite
Tectonic melange
Magmatic Arc
Basement
KIRKUK EMBAYMENT
LURESTAN SALIENT
DEZFUL EMBAYMENT
Tigris River
Zagros Front
PERSIAN GULF
MRF
HZF
MFF
ZFF
KNF
MZRF
DF
SPF
SF
BF
MISF
WF
GPS Velocity Vectors
Imbricated Zone
Simply Folded Belt
Mountain Front Flexure
Foredeep Zone
Mesopotamia-Persian Gulf Foreland Basin
Reverse/Thrust Fault
Dextral Strike-slip Fault
Sinistral Strike-slip Fault
Normal Fault
Inferred Fault
Anticline Axis

Figure 3: a) Regional tectonic setting of the Zagros orogen. White arrows and the numbers show the convergence velocity of the Arabian plate relative to the Eurasia fixed frame (Nocquet, 2012). Faults are compiled and modified after Berberian (1995), Berberian and Yeats (1999), Bahroudi and Talbot (2003), Hessami et al. (2003), Nazari et al. (2013), de Lamotte and Leturmy (2013), and Fathian et al. (2016). UDMA: Urmia-Dokhtar Magmatic Arc. b) Map of the Zagros orogeny structural subdivisions (see text for details). Orange circles highlight the earthquake epicenters from the Iranian Seismological Center online bulletin (IRSC; http://irsc.ut.ac.ir) for the period 2006 to 2018 highlighting the nucleation of the earthquakes on the slabs and edges of the tectonic salients and recessions (i.e., Kirkuk embayment, Lurestan Arc, Dezful embayment and Fars arc). Dark grey ellipses represent the meizoseismal area of the documented earthquakes (Ambraseys and Melville, 1982; Berberian and Yeats, 2001; Berberian, 2014). Red vectors show GPS velocities relative to the stable Eurasia frame (Khorrami et al., 2019). BF: Borazjan Fault; BRF: Bala Rud Fault system; DF: Dehshir Fault; HZF: High Zagros Fault; KF: Kazerun Fault; KhF: Khanaqin Fault; MFF: Main Front Fault; MRF: MISF: Masjid-i-Soleyman Fault; Main Recent Fault; MZRF: Main Zagros Reverse Fault; SF: Surmeh Fault; SPF: Sabz Pushan Fault; WF: Widyan Fault; ZFF: Zagros Foredeep Fault. c) Seismotectonic context of the study area. Orange circles show the earthquake epicenters from the IRSC online bulletin for the period 2006 to 11 November 2017-the day before the Mw 7.3 Azgeleh earthquake. Green hexagons symbolize historical earthquake records (e.g., Ambraseys and Melville, 1982; Berberian and Yeats, 1999; Berberian, 2014) and the numbers in transparent rectangles represent the dates of the events. Black and red fault plane solutions indicate the earthquakes (1948-2017) from body waveform (Maggi et al., 2000; Talebian and Jackson, 2004; Nissen et al., 2011) and the Global Centroid Moment Tensor (GCMT; https://www.globalcmt.org) catalogs, respectively. Blue beach balls denote first motions focal mechanisms (Shirakova, 1967; McKenzie, 1972; Jackson and Fitch, 1981; Ni and Barazangi, 1986; Nissen et al., 2019). Red star marks the epicenter of the Azgeleh mainshock. Solid orange, blue and green rectangles indicate the location of the SAR image frames used for the coseismic

deformation of the Azgeleh, Tazehabad, and Sarpol-e Zahab events, respectively. The orange rectangle frames also represent the SAR dataset applied to retrieve the postseismic deformation.

Deformation in the Zagros is also accommodated along transverse faults. These deep-seated, basement-involved Pan-African structures have repeatedly displaced fold axes, and seismicity patterns (Figure 3b). Lateral displacement of the MFF (Figure 3b) is also a result of the reactivation of these strike-slip faults (Hessami et al., 2001) bounding the Lurestan and Fars salient (Alavi, 2007). The seismically active strike-slip faults are mostly the N-S trending ones reported in the western Fars Arc, such as the Kazerun and Borazjan faults (Figure 3b) (Hessami et al., 2001; Walpersdorf et al., 2006; Nissen et al., 2011). However, Hessami et al. (2001) suggest some of the Pan-African strike-slip faults are associated with few moderate- to large-magnitude earthquakes indicating these faults are aseismic and deformation along them occurs as creeping. The Khanaqin fault is one of these faults showing little historical and/or considerable instrumental seismicity in the Northwest Zagros (Figure 3b, c). The rightlateral Khanaqin fault together with the seismically active Bala Rud sinistral thrust fault system have displaced the MFF for more than 130 km and about 120 km and mark the boundary of the Lurestan Arc with the Kirkuk Embayment to the northwest and the Dezful Embayment to the southeast, respectively (Figure 3b) (Hessami et al., 2001; Alavi, 2007).

The Mw 7.3 earthquake of 12 November 2017, termed as the “Azgeleh event”, occurred on the boundary

of the Lurestan Arc and the Kirkuk Embayment (Figure 3c). The Azgeleh event is the largest instrumentally recorded earthquake in the Zagros orogen and, in other words, the largest seismically documented event ever in this region, although historical seismicity studies show the Silakhor earthquake of 1909 A.D. (Figure 3b, c) to be of the same order at M 7.3- 7.4 (Ambraseys and Melville, 1982; Berberian, 2014). Unlike in the other structural domains in the Iranian Plateau, such as the Alborz and Central Iran, the Zagros has experienced only two earthquakes of magnitude 7 and/or larger to date. The Saimareh event (Figure 3c), around 9000 BCE, is possibly another documented large-magnitude earthquake (>Mw 7.0) along the Zagros (Berberian, 2014).

The Azgeleh event has been termed differently in other studies as the Darbandikhan, Sarpol Zahab, Sarpol Zahāb, Ezgeleh, Ezgeleh-Sarpolzahab, Sarpol-e Zahab, and Kermanshah (Barnhart et al., 2018; Yang et al., 2018; Vajedian et al., 2018; Feng et al., 2018; Chen et al., 2018; Ding et al., 2018; Gombert et al., 2019; Nissen et al., 2019; Kuang et al., 2019). The large magnitude and the aftermath of the Azgeleh event have triggered much geoscientific research. Using Synthetic Aperture Radar (SAR) coherence analysis, Karimzadeh et al. (2018), Washaya and Balz (2018), and Olen and Bookhagen (2018) studied the damage to buildings and affected urban areas. Triggered landslides and rockfalls

as well as liquefaction were investigated by Interferometric Synthetic Aperture Radar (InSAR), coherence analysis, and field observations (Miyajima et al., 2018; Vajedian et al., 2018). Tavani et al. (2018) provided subsurface data of seismic reflection profiles and interpreted the geometry of the inferred faults within the hypocentral area of the Azgeleh event. The mainshock source model was also inferred by inversion of teleseismic, regional, and local data (Chen et al., 2018; Ding et al., 2018; Nissen et al., 2019) and near-field strong motions (Gombert et al., 2019). Many researchers produced abundant observations inferred from Synthetic Aperture Radar (SAR) data. Barnhart et al. (2018), Feng et al. (2018), Wang and Bürgmann (2018), Yang et al. (2018), and Fathian et al. (2019) investigated the coseismic and postseismic deformation and related source models using InSAR-based techniques. Yang et al. (2018), Vajedian et al. (2018), Tolomei et al. (2018), Wang et al. (2018), Chen et al. (2018), Ding et al. (2018), Kuang et al. (2019), Nissen et al. (2019), and Gombert et al. (2019) presented coseismic displacement maps and source parameters constrained by InSAR observations, resolving a roughly similar geometry of 14° to 18° dip at a focal depth between 13 and 18 km. Barnhart et al. (2018) proposed a model of a ramp-flat fault with a lower dip of 1°–5° for the up-dip afterslip.

The source geometry introduced in previous studies only covers the epicentral area of the mainshock, and little information is available on the eastern and southern regions of the retrieved mainshock fault, where an intense occurrence of the aftershocks exists. In this chapter, we expand the investigation beyond the epicentral area of the mainshock and to the aftershocks to identify whether these regions relate to the mainshock source and to explore other possible sources triggered by the mainshock and/or involved in the surface deformation. Another aim of this chapter is the relevance of the distribution and the concentrations of the seismic events around the Lurestan Arc and the Kirkuk Embayment boundary where an abrupt change in topography has characterized the margin; this will provide insights to understand better the exceptional occurrence of the large-magnitude Azgeleh event and the characteristics of the studied events. The mainshock was followed by more than 10,000 aftershocks (Ml > 0.4) from 12 November 2017 to April 2019, among which 17 events occurred with magnitude 5.0 or larger (Iranian Seismological Center: IRSC). On 25 August 2018, an Mw 5.9 occurred near the city of Tazehabad (herein termed as the "Tazehabad event"), 45 km to the east of the Azgeleh epicenter, and one year after the Azgeleh earthquake, an Mw 6.3 struck the city of Sarpol-e Zahab (herein termed as the "Sarpol-e Zahab event") on 25 November 2018. The majority of the large aftershocks,

including the Tazehabad and Sarpol-e Zahab events, are associated with strike-slip focal mechanisms (Global Centroid Moment Tensor: GCMT), and the epicenter of the largest aftershocks are located within the different alignments of the aftershocks.

We firstly document the earthquake data recorded from a dense local seismic stations network deployed after the Azgeleh event and subsequently relocate the selected records utilizing the double-difference earthquake location technique (Waldhauser, 2000). We study the coseismic permanent displacement of the Azgeleh, Tazehabad, and Sarpol-e Zahab events. Next, we acquire the postseismic deformation of the epicentral area of the 2017–2018 seismic sequence and analyze the complexity of the faults involved in the seismic sequence as well as their contribution to the postseismic phase. We use two-pass and multi-temporal interferometric techniques-i.e., Differential SAR Interferometry (DInSAR) and Small BAseline Subset (SBAS) methods—to study the coseismic and postseismic deformation fields of the earthquakes in the region, respectively. To retrieve the source parameters for coseismic and postseismic deformation, we used non-linear and linear optimization algorithms to find the best-fit data source; InSAR observations were modeled introducing seismological and tectonic constraints, as described in detail in Sections 3.4 and 3.5. We also use the Coulomb Failure Function (CFF) to estimate the

stress change caused by the Azgeleh event on the previously mapped faults and the recently retrieved sources within the epicentral area of the seismic sequence. In this chapter, the Azgeleh, Tazehabad and Sarpol-e Zahab events refer to individual earthquakes, and the Azgeleh, Tazehabad, and Sarpol-e Zahab faults pinpoint sources retrieved via modeling of the InSAR observations of these events.

We introduce, for the first time, a set of faults involved in the 2017–2018 seismic sequence in western Iran including: a duplex (flat-ramp-flat) fault structure, an east-striking sinistral tear fault, as well as a north-striking and a northeast-striking dextral strike-slip faults, all of which have been seismically active right after the mainshock and involved in the postseismic phase. We present afterslip along the retrieved sources and up-dip and down-dip afterslip on the mainshock source fault. We show the interaction of the faults' activity with the morphology and topography of the ZFTB on the frontal edge of the Lurestan Arc. The location of the previously mapped faults in the Zagros is speculative and inferred; accordingly, large misfits with InSAR observations could be observed. We compiled, modified, and mapped the faults within the study area to reduce the misfits and obtain a more detailed and precise location of the faults in order to analyze the role of the available structures in the deformation of the 2017– 2018 western Iran seismic sequence.

4 Active on- and offshore tectonics in the Bushehr area (Zagros, SW Iran)

Abstract

This study focuses on the tectonically active structures within the Bushehr area, SW Iran, using tectonic geomorphology, remote sensing, and Quaternary geochronology. In addition, 2D seismic-reflection data were interpreted, imaging active subsurface structures offshore in the Persian Gulf. Reviewing the Chahpir, Abtavil, and Mand anticlines, we investigate in detail both the onshore and offshore Quaternary evolution of the Bushehr anticline as the frontal-most tectonically active structure in the Bushehr Peninsula. We identified, mapped, and documented at least two generations of uplifted marine terraces that show lateral elevation decrease from the anticline apex. The older terrace (Terrace-I) dates from ca. 32 ka BP and is ca. 25 m APSL, while the younger (Terrace-II) dates from ca. 3.7 ka BP and is only ca. 1.4 m APSL, proposing a local uplift rate of ca. 0.8 mm/yr across the Bushehr Peninsula. We introduce the Bushehr, Abtavil, and North Bushehr active faults as well as a fault branch -the Kharg Mish fault- aligned with the N-S-trending Kharg fault, associated with the Bushehr anticline axis. The ca. 16 km long Abtavil anticline, located in the northeast of the city of Bushehr, is associated with the Abtavil and North

Bushehr faults. The North Bushehr Fault has displaced Quaternary deposits, where the young unit is emplaced between the old and older units. Ongoing deformation in the study area is documented by offshore 2D seismic-reflection data that show the development of a recent sedimentary depocenter offshore of the Bushehr Peninsula. The seismic-reflection data show evidence for syndepositional recent folding, defining the presentday deformation along the Zagros orogenic front in the Persian Gulf. Similar observations are also documented in the active offshore Mand syncline adjacent to the onshore Mand anticline with a consistent trend. Seismic interpretations characterize active folding of the Bushehr anticline and the offshore Mand syncline since ca. 600 ka BP as a minimum. Integrated on- and offshore geological analysis indicates that the congruent bending of the northern hinges of the Mand syncline, and the Bushehr and Mand anticlines, can be linked to active shortening accompanied by slip partitioning in the Qatar syntaxis along the roughly N-S trending, PanAfrican transverse faults. The study area provides a textbook example, imprinting contemporaneous incipient deformation and syn-kinematic sedimentation.

4.1 Introduction

The Zagros orogen is characterized by an array of tectonic recessions and salients (Figure 4a) consisting from northwest to southeast of the Kirkuk Embayment, the Lurestan Arc, the Dezful Embayment, and the Fars Arc outlined by the transverse Pan-African faults-e.g., the Khanaqin, Bala Rud, and Kazerun faults (Berberian, 1995; Hessami et al., 2001; Alavi, 2007; Fathian et al., 2021). Some salt diapirs are attributed to the N-S-oriented dextral transverse faults in the central Zagros, such as the Kazerun and Borazjan faults, forming the Kazerun-Qatar and Mangarak-Marzuk lineament (Figure 4b) (Kent, 1979; Talbot and Alavi, 1996; Koyi et al., 2008).

The Bushehr area (including the Bushehr Peninsula) lies in the very southwestern boundary of the Fars Arc and the Dezful Embayment (Figure 4b) in the central Zagros. Multiple, moderate-sized historical and instrumental earthquakes, such as the 1824 (Ms > 6.0), 1986 (Ms 5.5), and 1988 (Ms 5.8) A.D. (Ambraseys and Melville, 1982; Berberian, 2014), are associated with the Kazerun fault system, including the Kazerun and Borazjan faults (Figure 4b). However, low- to moderate-sized historical and/or instrumental earthquakes are less frequent within the Bushehr area, where few active structures have been reported.

In this study, we investigate, review, and introduce the tectonically active structures within the Bushehr area (Figure 4). We focus on the onshore and offshore of the Bushehr area to study the tectonically active structures and explore the link between the active structures and the present-day morphology. Using optical satellite imagery and field observations, we provide a detailed Quaternary geological map of the area. In addition, using sedimentary classifications, geomorphological approaches, real-time kinematic (RTK) GNSS/GPS surveys as well as Optically Stimulated Luminescence (OSL) and radiocarbon (14C) dating techniques, we identify, describe, interpret, and date the tectonically active features within the Bushehr area. Through interpretation of offshore 2D seismic-reflection data, we outline the offshore active structures and resolve the structural and kinematic connections between the onshore and offshore structures.

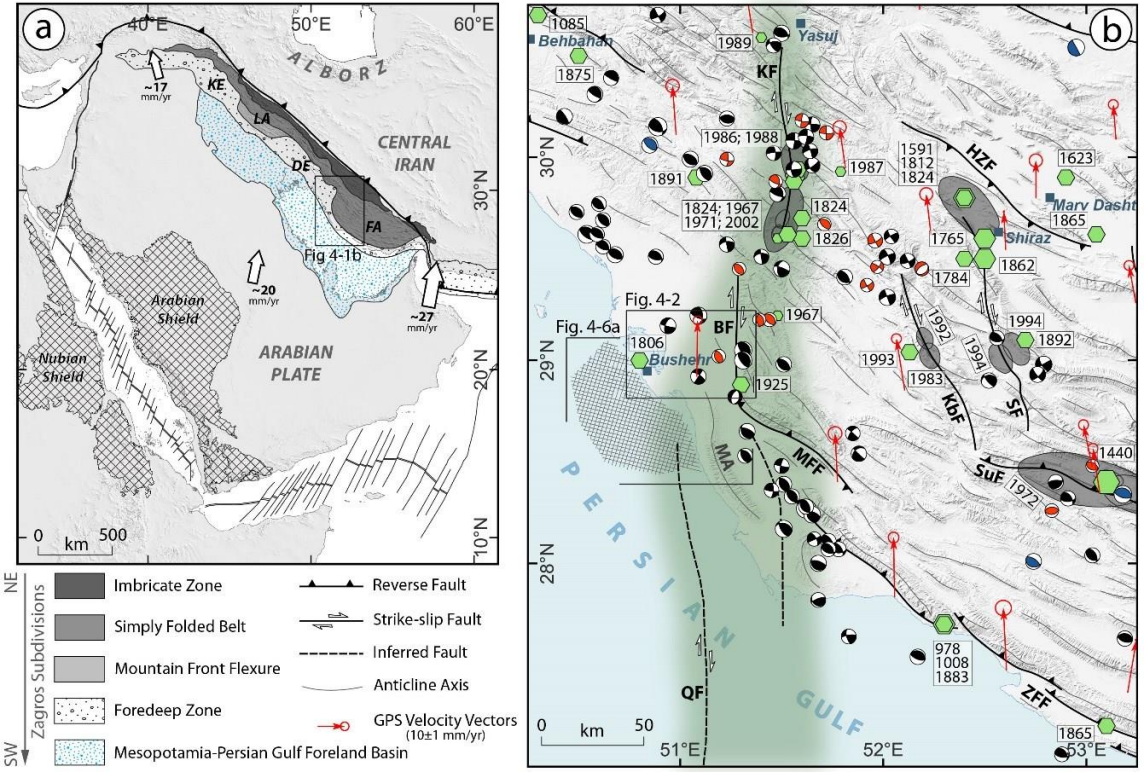
a
40°E
50°E
60°E
30°N
20°N
10°N
ALBORZ
CENTRAL IRAN
KE
LA
DE
FA
Fig 4-1b
~17 mm/yr
~20 mm/yr
~27 mm/yr
Arabian Shield
Nubian Shield
ARABIAN PLATE
0 km 500
NE
SW
Zagros Subdivisions
Imbricate Zone
Simply Folded Belt
Mountain Front Flexure
Foredeep Zone
Mesopotamia-Persian Gulf Foreland Basin
Reverse Fault
Strike-slip Fault
Inferred Fault
Anticline Axis
GPS Velocity Vectors (10±1 mm/yr)
b
1085
Behbahan
1875
1989
Yasuj
KF
1986; 1988
1987
1891
1824; 1967
1971; 2002
1824
1826
1591
1812
1824
HZF
1623
Mary Dasht
1865
1765
Shiraz
1862
1784
Fig. 4-2
Fig. 4-6a
1806
Bushehr
BF
1967
1925
1992
1994
1993
1983
1994
1892
KbF
SF
MA
MFF
SuF
1972
1440
PERSIAN GULF
978
1008
1883
ZFF
1865
QF
30°N
29°N
28°N
0 km 50
51°E
52°E
53°E

Figure 4: a) Tectonic setting of the Arabia-Eurasia collision illustrating the sub-domains of the Zagros orogen (modified after Fathian et al., 2021). White arrows exhibit the convergence velocities (Nocquet, 2012) relative to a fixed Eurasia frame. KE: Kirkuk Embayment; LA: Lurestan Arc; DE: Dezful Embayment; FA: Fars Arc. b) Seismotectonic configuration of the southwestern Zagros. Faults are compiled and modified after Fathian et al. (2021) and references therein. Grey ellipses are the documented meizoseismal areas of the seismic events, and the green hexagons represent the historical earthquakes (e.g., Ambraseys and Melville, 1982; Berberian, 2014). Black, blue, and red beach balls denote the fault plane solutions from the Global Centroid Moment Tensor (GCMT; https://www.globalcmt.org), first motions (Jackson and McKenzie, 1984; Ni and Barazangi, 1986), and Swiss Seismological Service (ZUR-RMT; http://www.seismo.ethz.ch) catalogs, respectively. Red arrows indicate GPS velocities in a Eurasia fixed reference frame (Khorrami et al., 2019). Transparent green polygon demonstrates the Kazerun-Qatar lineament zone outlining the incipient Qatar syntaxis (modified after Talbot and Alavi, 1996). Black lines network in the Persian Gulf illustrates the offshore 2D seismic lines (NIOC). BF: Borazjan Fault; HZF: High Zagros Fault; KbF: Karehbas Fault; KF: Kazerun Fault; MA: Mand Anticline; MFF: Main Front Fault; QF: Qatar-South Fars Fault; SF: Sabzpushan Fault; SuF: Surmeh Fault; ZFF: Zagros Foredeep Fault.

A particular focus of this study is on the tectonically active Bushehr and Abtavil anticlines (Figure 5) concerning the Quaternary uplift of these structures associated with active faulting. We study the uplifted marine terraces in the Bushehr Peninsula and show their chronological relationship with the growth of the Bushehr anticline. We furthermore quantify the slip rate of active faults using OSL and radiocarbon dating across the study area. The study finally documents the dynamic linkage between tectonically active offshore synclines and anticlines and onshore trends of folding and faulting. We integrate on- and offshore analysis to show the interaction of early-stage tectonic activity of structures across the Zagros deformation front.

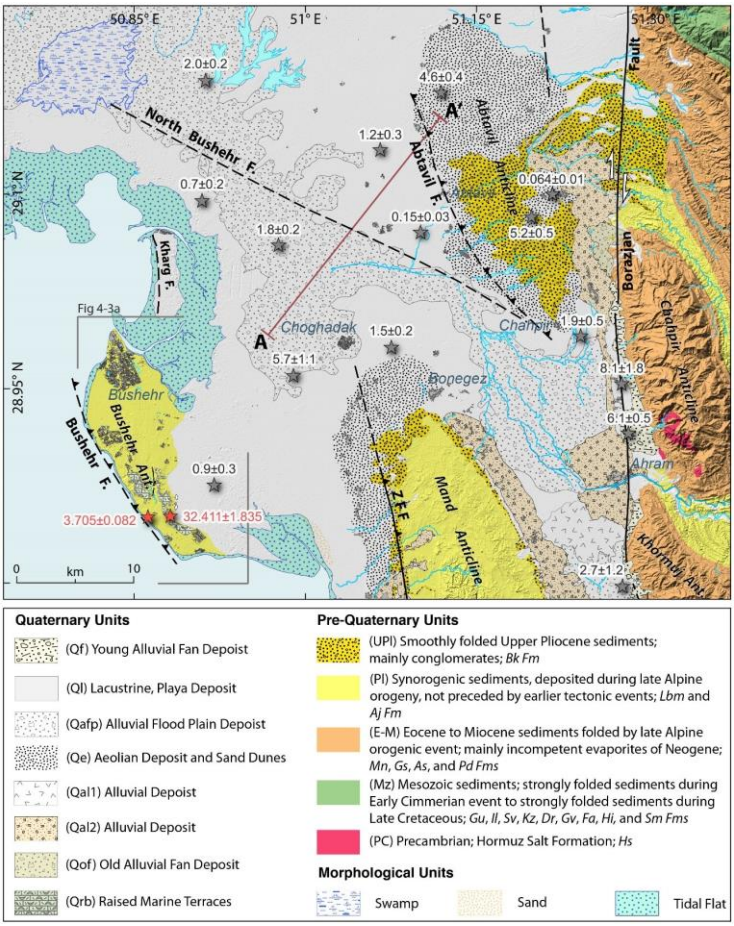

Figure 5: Map showing the geologic and morphologic units of the study area. Black stars represent the OSL dating values and the red stars indicate the radiocarbon ages from the marine terraces. The values are in ka BP. See Figure 6 for the AA′ profile. ZFF: Zagros Foredeep Fault; Fm: Formation; Bk: Bakhtiari; Lmb: Lahbari Member; Aj: Aghajari; Mn: Mishan; Gs: Gachsaran; As: Asmari; Pd: Pabdeh; Gu: Gurpi; Il: Ilam; Sv: Sarvak; Kz: Kazhdumi; Dr:

Dariyan; Gv: Gadvan; Fa: Fahliyan; Hi: Hith; Sm: Surmeh; Hs: Hormuz Series.

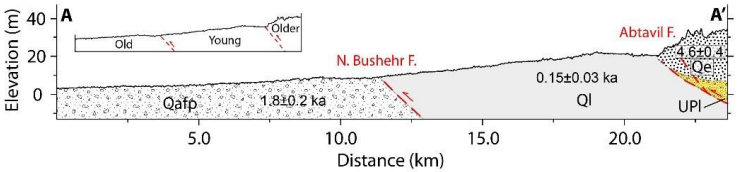

Figure 6: Schematic profile across the North Bushehr and Abtavil faults utilizing the Copernicus GLO-30 DEM (see Figure 4-2 for the location of the profile). Ql unit—the lacustrine and playa deposits—is located between two older units of aeolian deposits (Qe) to the northeast and the alluvial flooded plain deposits (Qafp) to the southwest. Inset sketch indicates the deposits are not chronologically in order; the young deposits have been emplaced between the old and older deposits due to the movements of the active faults.

5 Shallow deformations within the coastal Zagros; insights from InSAR, seismic, and morphological data

Abstract

The Zagros orogen accommodates intense seismicity due to the ongoing deformation. However, outcropping faults are rarely observed and/or

documented. The earthquakes of Furg (November 6th, 1990) and Qir-Karzin (April 10th, 1972) are unique events, which are associated with a surface rupture in the Zagros Fold-and-Thrust Belt (ZFTB). The study of seismic cycle deformation within a region is of high significance to have a better understanding of the kinematic behavior of a seismogenic fault. We use two-pass differential Synthetic Aperture Radar Interferometry (DInSAR) to process the C-band RADARSAT-2 images to study the coseismic deformation of the Mw 6.3 Shonbeh earthquake of 9 April 2013. Utilizing the Small Baseline Subset (SBAS) method, we process a large number of X-band, COSMO-SkyMed images to measure the postseismic deformation field due to the Shonbeh event. We implement the Hypocenter program to relocate 3553 recorded aftershocks by our temporary local seismic network in the month following the mainshock. We additionally determine 53 fault plane solutions for the locally recorded aftershocks, indicating both reverse and strike-slip components. Exploiting the available SAR dataset from the beginning of 2013 to mid-2014, we observe the concentration of the deformation along at least two NW-striking zones arranged in a right-step pattern and parallel to the trend of the folds. The spatial and hypocentral distribution of the locally recorded earthquakes denotes the nucleation of the aftershocks along six NW-SE trending clusters, where the inferred, associated faults dip to SW and NE.

Two other N-S clusters of sub-vertically aligned hypocenters appear to associate with strike-slip motion. Non-linear and linear inversions of the coseismic deformation as well the hypocentral nucleation of the aftershocks indicate the distribution of the coseismic slip along at least two NW-SE trending segments aligned in a right stepping pattern, where the NW and SE segments dip to the southwest and northeast, respectively. We also use tectonic geomorphology and paleoseismology to document a previously unknown outcropped fault within the Zagros. This ~20 km fault zone lies between the Khormuj and Khaki anticlines, where the Simply Folded Belt (SFB) of the Zagros is physiographically known as the coastal Zagros. The Khormuj anticline, located in the northeast of the city of Khormuj, was previously linked to the Main Front Fault (MFF), which is running on the southern limb of the anticline. Further to the south, the oblique-slip Khormuj fault zone, which strikes roughly N120°, cuts the Quaternary sediments and displaced streams and ridges laterally and vertically. Opposite to the NE-ward dip of the MFF, the Khormuj fault dips to the southwest -approximately 75°- where the southern block is uplifted, marking the trace of the fault on the ground. Our field surveys and RTK GNSS/GPS observations indicate significant dextral strike-slip displacement compared to the dip-slip offset. We observe a sequence of fluvial risers in three different levels along the Khormuj fault. Observations from a

paleoseismological trench perpendicular to the Khormuj fault scarp evidence signatures of at least two paleoearthquakes. The Optically Stimulated Luminescence (OSL) age of the bottom of the colluvium wedge correlated with the older event indicates the latest event to be younger than 25±8 ka considering the fault cuts these deposits up to the surface.

5.1 Introduction

The external part of the generally NW-SE-oriented Zagros Mountains, known as the Zagros Fold-Thrust Belt (ZFTB), lies between the Mesopotamia-Persian Gulf Foreland Basin to the southwest and the High Zagros Zone (HZZ) to the northeast separated by the Zagros Foredeep Fault (ZFF) and the Main Front Fault (MFF), respectively. The ZFTB consists of the Zagros Foredeep Zone, the Mountain Front Flexure Zone, and the Simply Folded Belt (SFB) (Falcon, 1974; Berberian, 1995; Bahroudi and Koyi, 2003, 2004; Alavi, 2007). The ZFTB includes four physiographic provinces: from northwest to southeast, the Kirkuk Embayment, the Lurestan Arc, the Dezful Embayment, and the Fars Arc (Stöcklin, 1968; Bahroudi and Koyi, 2004; Alavi, 2007).

The Zagros accommodates approximately one-third to one-half of the measured ArabiaEurasia convergence (22±2 mm/y) (e.g., Vernant et al., 2004; Masson et al., 2005) forming one of the active and most

rapidly deforming orogen globally. The SFB, as the southern/ southwestern subdomain of the ZFTB, accommodates ~5–10 mm/yr of the active shortening (Hessami et al., 2006; Walpersdorf et al., 2006). The seismicity in the Zagros is distributed across an approximately 200 km wide zone exhibiting low-to moderate-sized earthquakes within the depths ranging from 8 to 14 km (Jackson and Fitch, 1981; Ni and Barazangi, 1986; Baker et al., 1993). An earthquake of Mw 6.3 (herein termed as the Shonbeh event) hit the Shonbeh area in southwestern Iran. The epicentral area of the earthquake and the distribution of the following aftershocks cover an area on the frontal edge of the Zagros Simply Folded Zone, southwestern Iran, between the Kaki and Kangan anticlines (Figure 7).

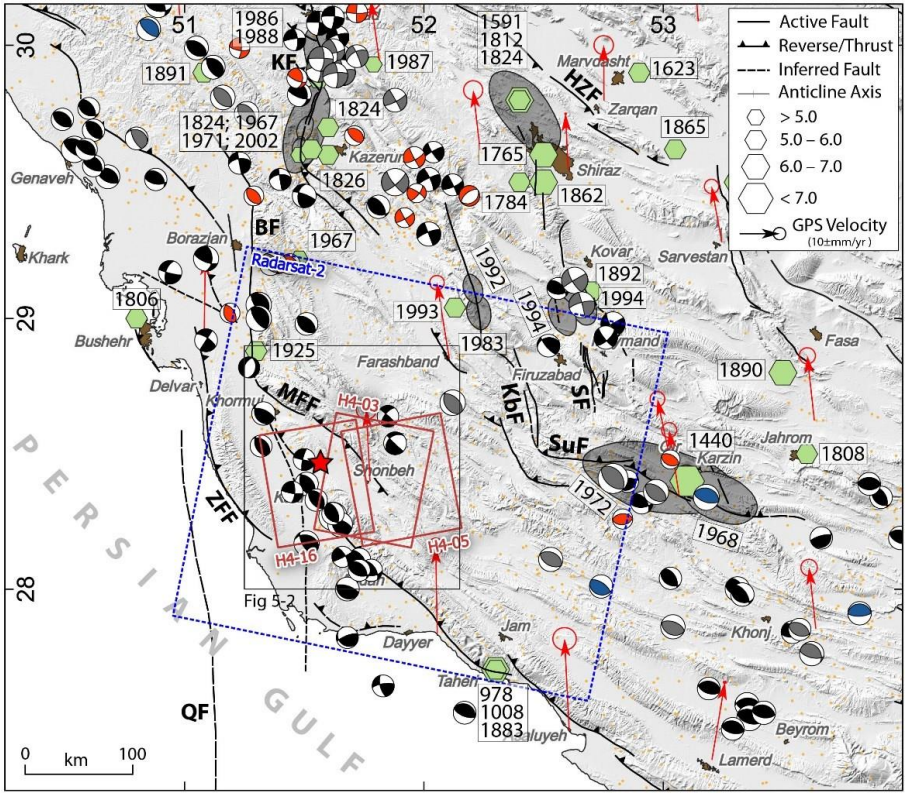
51
52
53
30
29
28
1986
1988
1891
KF
1987
1824
1824; 1967
1971; 2002
Kazerun
1826
1591
1812
1824
Marvdasht
1623
HZF
Zarqan
1865
1765
Shiraz
1784
1862
Genaveh
Khark
Borazjan
BF
1967
Radarsat-2
1992
1994
Kovar
Sarvestan
1892
1994
1806
1993
1983
Bushehr
1925
Farashband
Fasa
1890
Delvar
Shormu
MFF
H4-03
KbF
SF
Firuzabad
SuF
1440
Jahrom
Karzin
1808
Shonbeh
ZFF
1972
1968
H4-16
H4-05
Fig 5-2
Jam
Khonj
Dayyer
Taheri
978
1008
1883
Beyrom
Lamerd
QF
PERSIAN GULF
0
km
100
Active Fault
Reverse/Thrust
Inferred Fault
Anticline Axis
> 5.0
5.0 – 6.0
6.0 – 7.0
< 7.0
GPS Velocity
(10±mm/yr)

Figure 7: Seismotectonic configuration of the Fars Arc in the Simply Folded Belt (SFB) of the southwestern Zagros. Red star denotes the epicenter of the Mw 6.3 Shonbeh earthquake of April 9th, 2013 (IRSC; http://irsc.ut.ac.ir). Dashed blue rectangle shows the frame of the RADARSAT-2 images used to calculate the coseismic deformation of the Shonbeh earthquake. Red rectangles outline the frames of the COSMO-SkyMed SAR dataset applied for the postseismic phase of the event. Green hexagons and dark grey ellipses highlight the historical earthquakes and meizoseismal areas of the documented events, respectively (Ambraseys and Melville, 1982; Berberian and Yeats, 1999, 2001; Berberian, 2014). Black, grey, blue, and red beachballs symbolize the earthquakes from the Global Centroid Moment Tensor (GCMT; https://www.globalcmt.org), body waveform (Maggi et al., 2000; Talebian and Jackson, 2004; Nissen et al., 2011), first motion (Shirakova, 1967; McKenzie, 1972; Jackson and Fitch, 1981; Ni and Barazangi, 1986), and Swiss Seismological Service (ZUR-RMT; http://www.seismo.ethz.ch) catalogs, respectively.

Active fault mapping in the Zagros is mainly speculative and inferred (e.g., Fathian et al., 2021) due to the weak surface signature of faulting (e.g., Talebian and Jackson, 2004) as well as the large errors for the epicenter and depths of the earthquakes in the catalogs (e.g., Karasözen et al., 2019). Moreover, the historical earthquake records (e.g., Ambraseys and Melville, 1982) in Zagros are much fewer in number relative to the other seismotectonic provinces in Iran. In this study, we use multiple approaches to introduce previously unknown active faults as well as to compile and modify the previously mapped faults with a more precise location and lower misfits. To study the parameters of the

responsible sources for the Shonbeh earthquake, which can provide important information on the kinematic behaviors along this part of the coastal Zagros, we use Interferometric Synthetic Aperture Radar (InSAR) data acquired from C-band RADARSAT-2 as well as the 16-month X-Band COSMO-SkyMed dataset to retrieve the correspondent coseismic and postseismic deformation fields, respectively. We apply a standard slip inversion to recover the source parameters of the associated fault(s). We additionally relocate the aftershocks recorded by our local seismic network installed five days after the mainshock using the double-difference method (Waldhauser, 2000), and present 53 fault plane solutions of the aftershocks.

Termed as the Khaki-Shonbe earthquake, Elliott et al. (2015) have earlier studied the coseismic deformation of the Shonbeh event using the InSAR and seismic data. Considering only two scenarios of SW- and NE-dipping sources, they propose two along-strike, SW-dipping fault segments. Merging the relocated earthquakes with multiple scenarios of the source models, we propose different attributes for the Shonbeh coseismic sources different from that of Elliott et al. (2015). Furthermore, we infer and introduce a complex fault setting, including reverse and strike-slip faults, involved in the Shonbeh seismic sequence.

In this study, we also use tectonic geomorphology, paleoseismology, RTK GNSS/GPS surveys, and data from a paleoseismological trench perpendicular to the Khormuj fault scarp, to investigate the nature and kinematics of this previously unknown outcropping fault located at the deformation front of the Zagros fold-and-thrust belt.

6 Transient aseismic slip following the 2017 Mw 7.3 Sarpol-e Zahab earthquake: Possible evidence for fault frictional heterogeneity and thin-skinned shortening following a thick-skinned basementinvolved faulting in the Zagros fold-thrust belt

Abstract

We use interferometric synthetic aperture radar (InSAR) observations to investigate the fault model and afterslip evolution within 3 years after the 2017 Sarpol-e Zahab, Iran, Mw 7.3 earthquake. The anti-listric fault which is very similar to flat-and-ramp structure inverted by kinematic afterslip models is proposed to simulate the coseismic slip and afterslip evolution.

Compared with listric faults, linear inversions demonstrate that a planar fault can explain the oseismic deformation well enough. However, the stress perturbations caused by this basement-involved faulting propagated upward to the sedimentary cover. The transition of sedimentary cover-basement interface inferred by afterslip models is at a depth of ~13 km in the seismogenic zone, which coincides with the regional stratigraphic profile and indicates that the significant afterslip updip of the coseismic rupture is mainly controlled by frictional properties. We additionally find that the postseismic deformation is dominated by afterslip while the viscoelastic response is negligible with the best-fitting viscosity, which is of the order of 1019 Pa s. Compared to the best-fitting kinematic afterslip model, the stress-driven afterslip model tends to underestimate early postseismic deformation to the west, which may indicate the spatial heterogeneity of the frictional property of the fault plane. Because the coseismic rupture propagated along a basement-involved fault while the postseismic slip was likely to activate the frontal structures and/or shallower detachments in the sedimentary cover, the 2017 Sarpol-e Zahab earthquake may act like a typical event that contributes to both of the thick- and thin-skinned shortening of the Zagros in both seismic and aseismic way.

6.1 Introduction

The ongoing collision between the Eurasian and Arabian Plate has led to the formation of one of the most tectonically and seismically active intra-continental orogens: the northwestsoutheast striking the Zagros Mountains in southwestern Iran. The convergence velocity between the Eurasian and Arabian Plates is ~2 to 3 cm/yr, almost half of which is accommodated by the Zagros Mountain belt (Figure 6-1a; e.g., Vernant et al., 2004; Khorrami et al., 2019). In northwestern Zagros, the deformation rate is partitioned as ~5 mm/yr of dextral strike-slip motion along northwest-southeast trending faults and ~4 mm/yr of shortening perpendicular to the mountain belt, while in southeastern Zagros the deformation is ~9 mm/yr pure shortening perpendicular to the belt (Walpersdorf et al., 2006).

Contemporary active deformation around the Zagros Fold-Thrust Belt (ZFTB) is mainly derived from seismic and aseismic deformation triggered by thrust and strike-slip faulting (e.g., Barnhart and Lohman, 2013; Motagh et al., 2015; Copley et al., 2015), folding and uplift of sedimentary cover (e.g., Berberian, 1995), and ductile thickening of the basement (Allen et al., 2013). The Phanerozoic sedimentary cover rock is ~8 to 13 km thick, overlaying the Phanerozoic crystalline basement. A lot of work has been done to explore thin- and thickskinned shortening related to the Phanerozoic sedimentary succession and deep basement faulting in

the Zagros belt (e.g., Falcon, 1969; Talebian and Jackson, 2004; Molinaro et al., 2005; Mouthereau et al., 2012). Moderate magnitude earthquakes (~M 5–6) are widely distributed in ZFTB, but the characterization and contribution of such seismicity in cover-basement interaction are still not fully understood (e.g., Talebian and Jackson, 2004; Nissen et al., 2011; Motagh et al., 2015; Copley et al., 2015). A Hormuz salt unit in the Fars Arc and shales in the Lurestan Arc due to the strong mechanical contrast between sedimentary cover and basement are suspected as a decoupling layer at the cover-basement interface (e.g., McQuarrie, 2004; Alavi, 2007), which may impede the propagation of fault ruptures to the surface in this region. Under such geological and tectonic environment, many blind thrust faults which cut through the sedimentary cover, grow in ZFTB, and contribute to the current topography of the Zagros. The major faults within ZFTB consist of the Main Recent Fault (MRF), the Mountain Front Fault (MFF), the High Zagros Fault (HZF), and the Zagros Foredeep Fault (ZFF) (Berberian, 1995; Figure 8b).

On 12 November 2017 at 18:18 UTC, an earthquake with a magnitude of Mw 7.3 and focal depth of about 21 km struck ~50 km north of Sarpol-e Zahab city, in Kermanshah province of western of Iran, which is also very close to Iran and Iraq border (Figure 8). The main event occurred along a shallowly east-dipping reverse fault with dextral components in the Lurestan

Arc of ZFTB and is the largest earthquake in this region since the instrumental records. Several ~M 6 earthquakes in the sedimentary cover followed the mainshock such as the 25 August 2018 Mw 5.9 event and 25 November 2018 Mw 6.3 event (Figure 8b). However, these two smaller aftershocks along steeply dipping dextral strike-slip faults may reveal the strain partitioning in the northwestern Zagros belt as the overall convergence direction between the Eurasian and Arabian Plate changes from orthogonal shortening in southeastern Zagros to oblique shortening in northwestern Zagros (e.g., Talebian and Jackson, 2004). The 2017 Sarpol-e Zahab mainshock is located in the crystalline basement, where the seismicity interactions between the sedimentary cover and basal basement due to the possible existence of the weak Hormuz shale as a decoupled layer is still an open question (e.g., Nissen et al., 2011; Barnhart et al., 2018; Wang and Bürgmann, 2020).

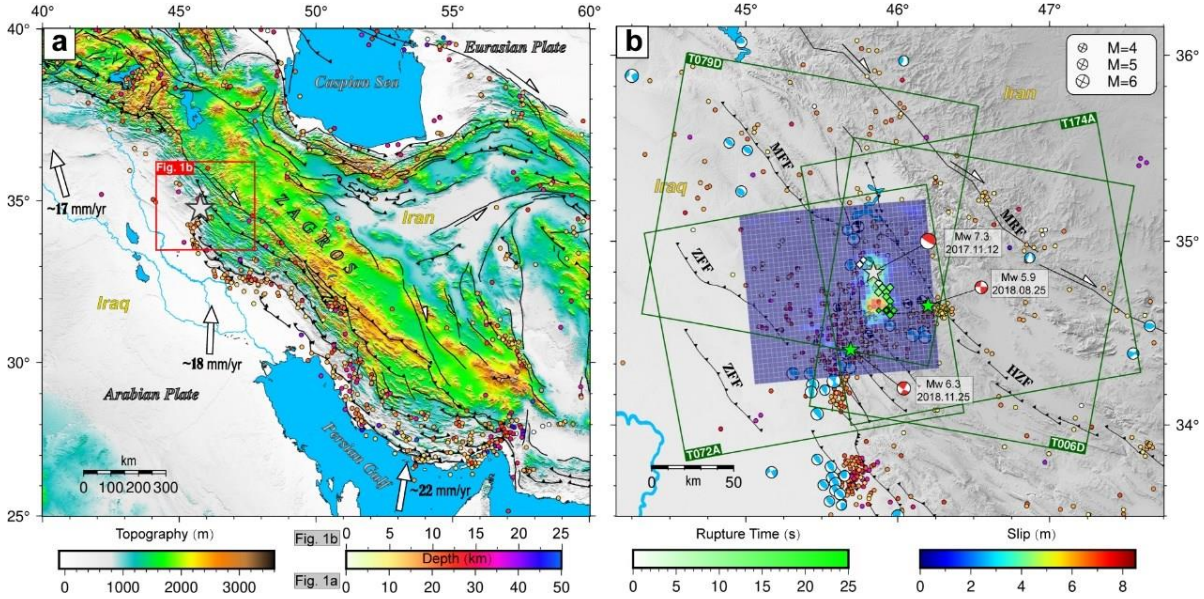
a
b
Eurasian Plate
Caspian Sea
Iran
Iraq
Arabian Plate
Persian Gulf
ZAGROS
Fig. 1b
~17 mm/yr
~18 mm/yr
~22 mm/yr
km
0 100 200 300
MFF
ZFF
HZF
T079D
T174A
T072A
T006D
M=4
M=5
M=6
Mw 7.3
2017.11.12
Mw 5.9
2018.08.25
Mw 6.3
2018.11.25
0 km 50
Topography (m)
0 1000 2000 3000
Fig. 1b
Fig. 1a
Depth (km)
0 5 10 15 20 25
0 10 20 30 40 50
Rupture Time (s)
0 5 10 15 20 25
Slip (m)
0 2 4 6 8

Figure 8: a) Tectonic background of the 2017 Sarpol-e Zahab earthquake. The colored dots are the earthquakes (from 1976 to 2021) from the Global Centroid Moment Tensor (GCMT) catalog (https://www.globalcmt.org). b) Detailed tectonic map of the seismogenic area. The blue beach balls are from the GCMT catalog. Colored dots are the earthquakes (from 2006 to 2021 with M > 3.5) from the Iranian Seismological Center (IRSC; http://irsc.ut.ac.ir). Dark green boxes indicate the spatial extent of the Sentinel- 1 imagery used in this study. The coseismic slip distribution is given with the anti-listric fault model. Black beach balls are from Nissen et al. (2019). Red beach balls are the focal mechanisms of the 2017 Sarpol-e Zahab mainshock and two smaller aftershocks. The green rhombuses represent the rupture time of the mainshock, which is mapped after Nissen et al. (2019). ZFF: Zagros Foredeep Fault; MRF: Main Recent Fault; HZF: High Zagros Fault; MFF: Mountain Front Fault.

Several studies have been done for a better understanding of seismic and aseismic slip of the 2017 Sarpol-e Zahab earthquake using geodetic observations (e.g., Barnhart et al., 2018; Chen et al., 2018; Feng et al., 2018; Vajedian et al., 2018; Yang et al., 2018; Nissen et al., 2019; Wang and Bürgmann, 2020; Lv et al., 2020; Fathian et al., 2021), but some debate still remains. In this study, we extend earlier studies and investigate both co and postseismic models of the 2017 Mw 7.3 Sarpol-e Zahab event with interferometric synthetic aperture radar (InSAR) data. Firstly, we analyze the optimal coseismic fault model from planar and a range of listric faults with coseismic interferograms. Then we process ~3 years of Sentinel-1 data to derive the postseismic deformation

time series and study the fault geometry and transient aseismic slip evolution for the first 4, 7, 10, 12, 24, and 36 months after the mainshock. Finally, we discuss fault frictional heterogeneity, the reactivation of the Mountain Front Fault system, and shallower multiple detachments that were most likely triggered by the mainshock, given our inversion results and the structural geology background of the Zagros.

7 Source characteristics of the Fin doublet earthquake of 14 November 2021 (Mw 6.2 and Mw 6.3) utilizing InSAR and seismic data

Abstract

On 14 November 2021, a doublet earthquake (Mw 6.2 and Mw 6.3) struck Fin and the surrounding area in the southeastern termination of the Zagros fold-and-thrust belt, southern Iran. Utilizing the two-pass differential SAR Interferometry (InSAR) method, the coseismic deformation fields, retrieved from 12-day pairs descending and ascending Sentinel-1 as well as descending ALOS-2, demonstrate a displacement pattern of maximum 40 cm toward the satellite in the epicentral area. To study the high-frequency rupture characteristics

of the Fin doublet earthquake, we use a back-projection analysis and teleseismic *P*-wave data recorded by the European seismic stations, which can present important information on the kinematic and physical behaviors of the corresponding source(s). The back-projected results suggest a single event of Mw 6.0 for the foreshock (Mw 6.2), and two subevents for the Mw 6.3 mainshock, where the rupture propagates northwestward with a speed of approximately 1.3 km/s. The slip inversion from the InSAR analysis exhibits best fitting on an east-west trending (~263°), north-dipping (~71°) fault as well as an east-west trending (~84°), south-dipping (~15°) thrust with a maximum coseismic slip value of ~2 meters. The distribution of the subevents of the main events and the following aftershocks shows a better fit with the south-dipping source. Additionally, the south-dipping thrust conforms well with the development of the Handan and Khurgu anticlines as well as the geological setting of the area introduced in the previous studies.

7.1 Introduction

The Zagros Mountains are one of the youngest and most active orogenic belts in the world (e.g., Stöcklin, 1974), accommodating almost half of the Arabian and Eurasian plates' convergence rate (e.g., Vernant et al., 2004). The present-day shortening and ongoing deformation have resulted in intense seismicity

of low- to moderate-magnitude earthquakes predominantly distributed across the Zagros Simply Folded Belt (SFB) and the Zagros Imbricate Zone (ZIZ) (Berberian, 1995; Talebian and Jackson, 2004; Barnhart et al., 2013; Karasözen et al., 2019). The lower Cambrian Hormuz salt Formation decouples the crystalline basement from the 8– 10 km thick sedimentary cover in the SFB (O'Brien, 1957; Colman-Sadd, 1978; Berberian, 1995).

Two consecutive earthquakes of Mw 6.2 and Mw 6.3 (herein termed as the Fin doublet earthquake) hit the Fin region in southern Iran (Figure 9) at 15:37 (12:07 GMT) and 15:38 (12:08 GMT) local time, respectively. The shaking from the earthquakes triggered rockfalls and landslides on the slopes of the neighboring anticlines. However, no surface rupture was evident through the field investigations or in the remotely sensed data.

The Fin doublet earthquake occurred on the southeasternmost part of the Zagros Mountains, close to the border of Makran and Central Iran structural domains (Figure 9), where the Zagros tectonic sub-domain is known as the Simply Folded Belt (SFB; e.g., Alavi, 2007). The epicentral area is located between the Handun, Khurgu, and West Namak whaleback anticlines. The anticlines in the SFB are mainly controlled by active blind faults, namely the Main Front Fault (MFF), the High Zagros Fault (HZF), and the Zagros Foredeep Fault

(ZFF) (e.g., Berberian, 1995). The earthquakes of Hurmuz (1497, M 6.5), Bandar Abbas (1622), and Qeshm (1897, M 6.4) are significant historical events in the area (e.g., Berberian, 2014). Instrumental earthquakes of 1962 (M 5.4), 1963 (M 5.2), 1965 (M 6.0) have occurred on the HZF (Ambraseys and Melville, 1982), and ~40 km further to the west of the 2021 Fin doublet earthquake, the 2006 Fin seismic sequence (Roustaei et al., 2010) has occurred.

In this study, we apply a *P*-wave back-projection method (e.g., Ishii et al., 2005) on the teleseismic data, acquired from the European seismic stations, to investigate rupture details of the Fin doublet earthquake. Using AlOS-2 PALSAR and Copernicus Sentinel-1 space-borne Synthetic Aperture Radar (SAR) data, we also employ the standard differential SAR interferometry (DInSAR) technique to measure the coseismic deformation phase of the Fin doublet earthquake. We then apply a standard inversion to retrieve the best-fit sources and reproduce the characteristics of the sources. We introduce an ENE-WSW-trending (~84°) south-dipping (~15°) thrust fault corresponding with the mainshock recovered from the InSAR data and confirmed by the seismic analysis.

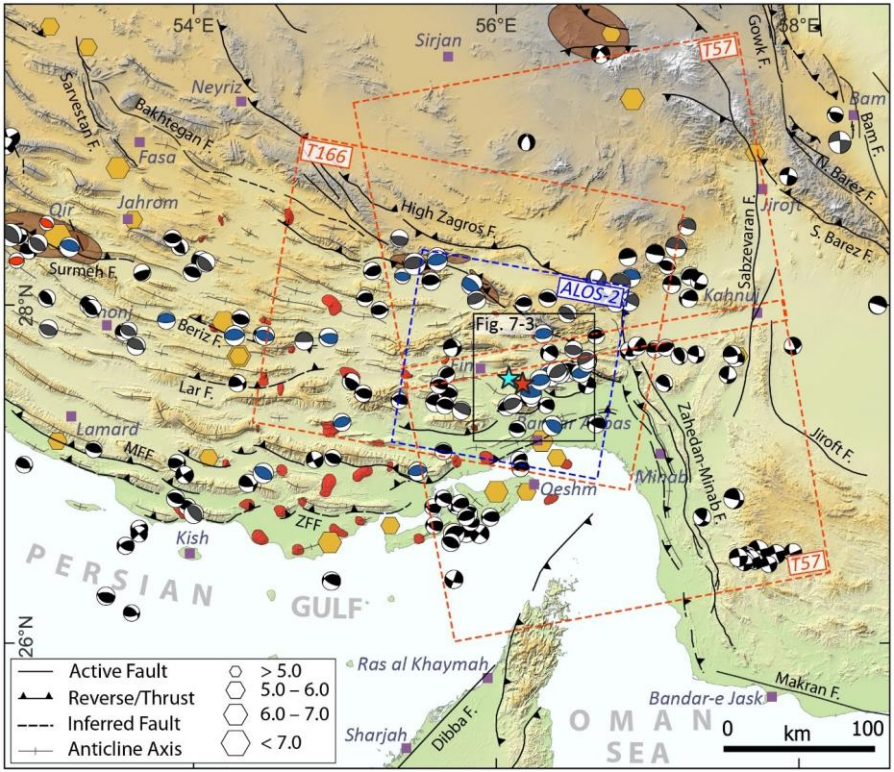
54°E
56°E
58°E
28°N
26°N
Sirjan
Neyriz
Sarvestan F.
Bakhtegan F.
Fasa
Jahrom
Qir
Surmeh F.
Beriz F.
Lar F.
Lamard
MFF
ZFF
Kish
T166
T57
High Zagros F.
ALOS-2
Fig. 7-3
Gowk F.
Bam
Bam F.
N. Barez F.
S. Barez F.
Jiroft
Sabzevaran F.
Kahnuj
Zahedan-Minab F.
Jiroft F.
Mihab
Qeshm
Ras al Khaymah
Sharjah
Dibba F.
Makran F.
Bandar-e Jask
PERSIAN GULF
OMAN SEA
Active Fault
Reverse/Thrust
Inferred Fault
Anticline Axis
> 5.0
5.0 – 6.0
6.0 – 7.0
< 7.0
0
km
100

Figure 9: Seismotectonic configuration of the southeastern termination of the Zagros fold-and-thrust belt, southern Iran. Light blue and red stars represent the foreshock (Mw 6.2) and the mainshock (Mw 6.3), respectively. Dashed blue and orange rectangles outline the ALOS-2 and Sentinel-1 images, respectively. Dark brown ellipses and orange hexagons indicate the meizoseismal areas of the documented earthquakes and the historical events, respectively (Ambraseys and Melville, 1982; Berberian and Yeats, 1999, 2001; Berberian, 2014). Black, grey, blue, and red beachballs denote the earthquakes from the Global Centroid Moment Tensor (GCMT; https://www.globalcmt.org), body waveform (Maggi et al., 2000; Talebian and Jackson, 2004; Nissen et al., 2011), and first motion (Shirakova, 1967; McKenzie, 1972; Jackson and Fitch, 1981; Ni and Barazangi, 1986) catalogs, respectively. Red polygons highlight the outcropped diapirs.

8 Synthesis

The results presented in this report contribute to identifying and characterizing multiple previously-unknown tectonically active structures within the Zagros as well as to understanding better the present-day regional kinematics of the Zagros orogen.

The arid to semi-arid climate and sparse vegetation within most of the study areas provide an exceptional environment to investigate using space- and air-borne active and passive data. Applying a standard slip inversion on the InSAR data (Chapter 3) that covers the epicentral area of the 2017–2018 Azgeleh seismic sequence in western Iran, we introduced the distribution

of the co- and postseismic slip along a set of faults of peculiar strikes, unlike the conventional NW–SE trend of the structures within the Zagros. Merging the InSAR observations with our locally recorded earthquakes, we optimized the geometry of the sources responsible for the co- and postseismic deformation fields of the Azgeleh earthquake and the following seismic sequence (Chapter 3) and proposed the coseismic slip of the mainshock distributed on a listric fault and the up-dip and down-dip afterslip developed onto the subhorizontal planes at ~5 and ~20 km describing the upper-crustal detachment and mid-crustal décollement within the epicentral area, respectively. Linear inversions of the InSAR data in Chapter 6 propose a planar source for the coseismic deformation of the Azgeleh event instead of the listric fault suggested in Chapter 3. Additionally, Chapter 6, unlike Chapter 3, presents only an updip afterslip for the postseismic phase. Despite a better misfit for the source in Chapter 6, the planar source cannot resolve well the downdip afterslip. Comparing these two chapters highlights the importance of studying earthquake cycle deformations using multidisciplinary approaches. The results and models in Chapter 6 are well-fitted and mathematically correct, confirming some other works (e.g., Barnhart et al., 2018; Wang and Bürgmann, 2020), which only rely on the InSAR observations as well. However, the models in Chapter 3 are refined according to the precise relocated

microseismic events of the seismic sequence. Integrating the seismic and InSAR observations provides a two-point solution to determine the source characteristics using better constraints. A similar approach was applied in Chapter 5 for the Shonbeh event to modify the sources associated with the Shonbeh seismic sequence.

The thin- and thick-skinned tectonics within the Zagros is yet under debate. The results presented in this thesis suggest an asymmetrical horizontal and vertical slip partitioning within the Zagros. Furthermore, the imbricated, duplex structure involved in the 2017–2018 seismic sequence characterizes the thick-skinned deformation in the Northwest Zagros, whereas some other works (e.g., Motagh et al., 2015) propose thin-skinned tectonics elsewhere in the Zagros. Previous studies on the Zagros deformation front (e.g., Oveisi et al., 2007) indicate no topographic evidence in the bathymetry of the Persian Gulf corresponding with evolving of the Mand detachment fold to a fault-bend fold (Sherkati et al., 2006). This thesis documents active offshore folds (Chapter 4) and shallow faults (see Section 9.1) in the Persian Gulf, verifying the transfer and propagation of the slip motions to more frontal structures in the marine parts (Figure 11).

The indentation morphology within the Zagros front is characterized by a sequence of the tectonic recessions and salients, physiographically known as the

Kirkuk Embayment, the Lurestan Arc, the Dezful Embayment, and the Fars Arc (Figure 11). The salients are outlined by sharp boundaries of reactivated basement-involved, Pan-African faults-the Khanqin, Bala Rud, and Kazerun-Qatar fault systems. The N-S-oriented Khanaqin and Kazerun-Qatar lineaments outline the abrupt topographic changes in the western boundaries of the Lurestan Arc and Fars Arc. Both lineaments diffuse farther to the south, where the deformation emerges at a low rate and in the early stages (e.g., Chapter 4). The 2017–2018 Azgeleh seismic sequence (Chapter 3) evidences seismic activity along the N-S Khanaqin lineament (Figure 11), previously known as a low seismic zone.

The Lurestan Salient is bounded by the dextral Khanaqin and sinistral Bala Rud faults, which allow southwestward extrusion of the block (Figure 10), developing escape tectonics in the Northwest Zagros. The western boundary of the Fars Salient, similar to the Lurestan Salient, is controlled by a dextral fault system—the Kazerun-Qatar fault system. The eastern edge, however, is not sharply outlined by a fault line, and the Fars Arc gets slender to the southeast. On the other hand, unlike the Lurestan Salient, the southeastern boundary is not characterized by a sinistral fault system, but the dextral Oman line (including the Dibba transform fault) is the principal structure that controls the southeastern side of the Fars Salient.

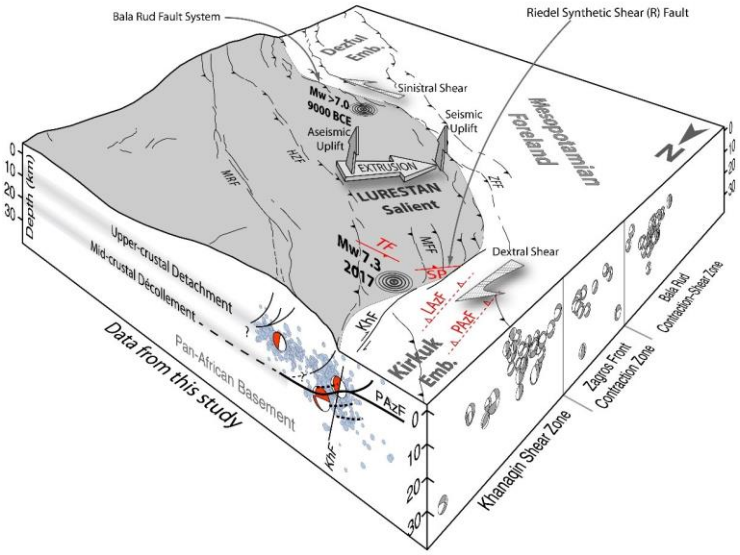

Figure 10: Schematic 3D block diagram showing indenter tectonics in the Northwest Zagros controlled by lateral extrusion of the Lurestan Salient along the Khanaqin and Bala Rud transverse faults. Aseismic deformation uplifts the inner Lurestan Arc and the seismicity is concentrated on the front and the edges of the boundary between the Lurestan Arc and the Mesopotamian foreland basin (including the Kirkuk and Dezful Embayments). Two of the largest earthquakes documented in the Zagros (concentric black circles), the Saimareh (~9000 BCE; Mw 7.0) and Azgeleh (12 November 2017; Mw 7.3) events, are analogically located on the slab of Lurestan Salient lateral boundaries. Solid red line and dashed red line with triangles represent the surface projection of the modeled faults in this study. Black solid lines are the compiled and modified faults. Light and dark grey 3D arrows denote the horizontal, southwestward extrusion of the Lurestan salient, and vertical strain partitioning in the Lurestan Salient; brittle deformation concentrates in the front while the inner parts uplift mainly aseismically. Hatched arrows show regional dextral and sinistral movements along the Khanaqin and Bala Rud shear zones, respectively. Blue circles represent the

relocated events in this study. Red beach balls indicate fault plane solutions of the Azgeleh, Tazehabad, and Sarpol-e Zahab events. Thick solid black lines in the section represent the faults from this study and the dashed black lines denote the inferred imbricate faults. Grey beach balls denote all fault plane solutions (see Figure 3-1c for references) within the study area. KhF, MFF, ZFF, HZF, and MRF are similar to the abbreviations in Figure 3-1; LAZF: Listric Azgeleh Fault; PAZF: Postseismic Azgeleh Fault; TF: Tazehabad Fault; SP: Sarpol-e Zahab Fault.

The 2017 Azgeleh event (e.g., Fathian et al., 2021) together with the Saimareh (9000 BCE) and 1906 Silakhor (e.g., Ambraseys and Melville, 1982) events are the merely documented earthquakes of magnitude 7.0 or larger in the Zagros, all of which have occurred in the Lurestan Arc/Salient. The events' meizoseismal areas are relatively located on three corners of the trapezoid-shaped Lurestan Arc (Figure 11), indicative of a possible absent event, in the same order, in the fourth corner. Nonetheless, finding evidence of such an event needs further investigations and field studies validation.

Surface faulting in the Zagros is exceptionally rare; both documented earthquakes associated with a surface rupture (i.e., the 1972 Qir-Karzin and 1990 Furg events) have occurred in the Simply Folded Belt (SFB). The surface expression of the identified Khormuj fault (Chapter 5), as well as the other surface ruptures, are aligned on a WNW-ESE lineament (Figure 11). The truncation across the Fars Arc, combined with the dextral movements, accommodated along the main fault systems

outlining the Fars Arc -the Main Zagros Recent Fault, the Khanaqin, Dibba, and Minab faults- is likely inducing internal counterclockwise rotations (Figure 11). The Fars, however, is a broad block, and the rotational movements within the inner parts diffuse, and most likely, the deformation concentrates on the shallower parts. We call this shallow band of deformation the Zagros Rupture Band (ZRB; Figure 11), where all of the outcropping faults (the Furg, Surmeh, and Khormuj faults) are aligned (Figure 11).

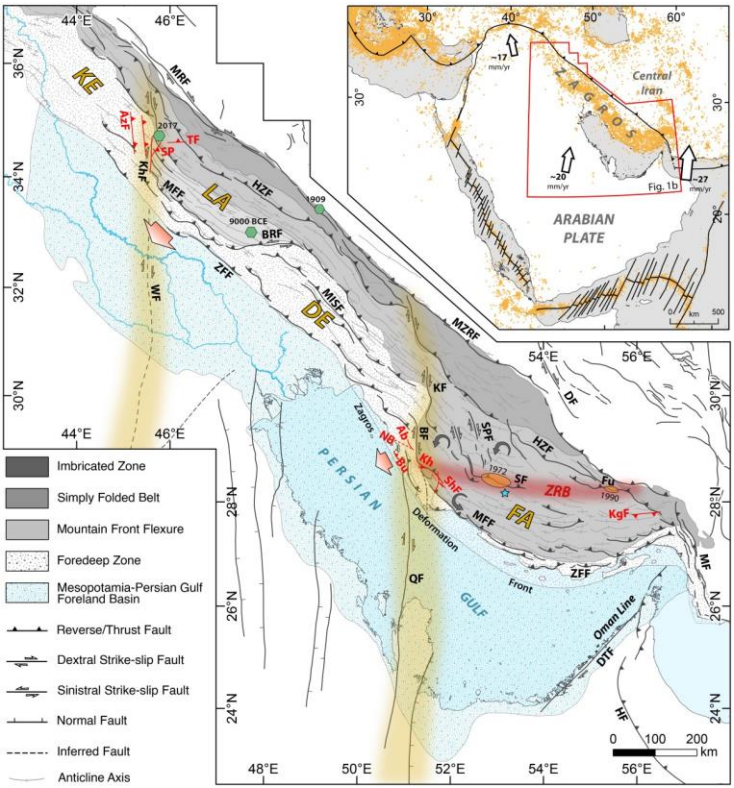

Figure 11: Tectonic framework and the subdomains of the Zagros orogen compiled and modified after Fathian et al. (2021) and the references therein. KE: Kirkuk Embayment; LA: Lurestan Arc; DE: Dezful Embayment; FA: Fras Arc. See Figure 3 and Figure 4 for the abbreviations in black (Fu: Furg Fault; MF: Minab Fault). Red lines demonstrate the active faults and earthquake sources introduced in this thesis. Ab: Abtavil Fault; AzF: Azgeleh Fault; Bu: Bushehr Fault; DaF: Darang Fault; KgF: Khurgu Fault; Kh: Khormuj Fault; NB: North Bushehr Fault; ShF: Shonbeh Fault; SP: Sarpol-e Zahab Fault; TF: Tazehabad Fault. Orange ellipses are the meizoseismal area of the Qir-Karzin (10 April 1972; Mw 6.7) and Furg (6 November 1990; Mw 6.5) earthquakes associated with surface

rupture (e.g., Berberian, 2014) and the transparent red polygon illustrates the Zagros Rupture Band (ZRB). Transparent orange polygons highlight the Khanaqin and Kazerun-Qatar lineaments. Green Hexagons denote the earthquakes of M7.0 or larger in the Zagros. The arrows with red gradient color indicate the propagation of the Zagros deformation front southwestward on to the Mesopotamian-Persian Gulf Foreland Basin. Blue star shows the epicenter of the Khonj shallow earthquake (Mw 4.9) of 6 January 2017 (see Section 9.3 for more details). Inset map demonstrates the Arabia-Eurasia collision. White arrows represent the GPS velocities of the Arabian plate relative to a stable Eurasia frame (Nocquet, 2012). Orange circles illustrate the earthquake epicenters for the period 1904 to 2013 from the reviewed International Seismic Centre (ISC; http://www.isc.ac.uk) bulletin.

9 Outlook

Despite the previous works (e.g., Motagh et al., 2015; Barnhart et al., 2018) as well as the data and analyses proposed in this study indicating concurrent deformation within the sediment cover and the basement in the Northwest Zagros, the thin- and thick-skinned tectonics within the Zagros yet remains under debate. The seismic versus aseismic deformation ratio across the Zagros orogen as the frontal portion of slip partitioning with respect to the Arabia-Eurasia convergence is not known to an adequate level. Further advanced InSAR, seismological, and geodetic investigations are required to

assess the seismic and aseismic quantities in the Zagros belt.

The seismogenic sources in the Zagros (likewise in Iran) as a crushed and earthquake-prone domain are not fully identified and quite a few recent earthquakes have occurred along the faults that were previously unknown/unmapped. The mechanisms and behaviors—e.g., seismic cycle deformation, slip rates, kinematics, and so on—for the majority of the active faults in this domain are not fully understood. The integration of the approaches applied in this thesis would properly address the abovementioned characteristics. The following sections present other case studies for which I launched the investigations, and acquired preliminary results and analyses. The studies, however, remained unaccomplished due to the pandemic situation; consequently, I could not manage to bring these studies into a publishable state.

9.1 Tectonostratigraphy of the Bushehr area

Numerous tectonostratigraphic studies across the Zagros have been performed (e.g., Sherkati et al., 2006; Alavi, 2007; Jahani et al., 2009). The offshore studies have been mainly focused on hydrocarbon investigations and little is known about the active tectonics of the Persian Gulf. In this thesis, I coupled the on- and offshore data to examine the tectonically active

structures in the Persian Gulf immediately adjacent to the Bushehr Peninsula. The application of these data with an active tectonic perspective in future studies across the Persian Gulf and the frontal Zagros is indisputably necessary.

The available NIOC seismic data for the Persian Gulf provide a satisfactory resolution for depths up to 3 km. The shallower depths, however, require different approaches that complement these data (Figure 12).

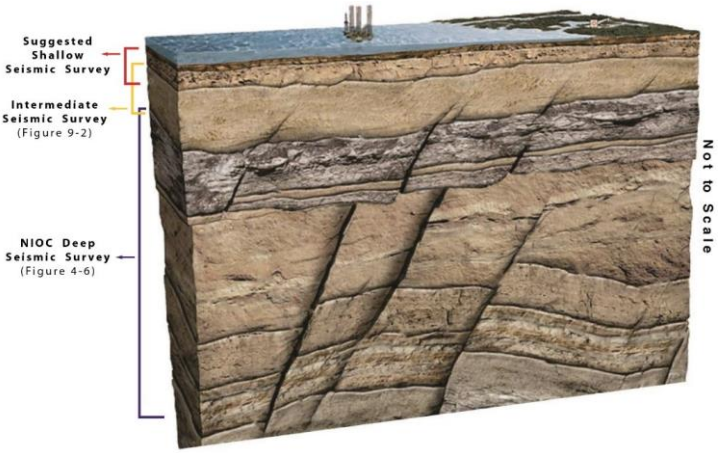

Figure 12: 3D schematic block of the offshore study area. Although the intermediate data complement the deep seismic data to detect the shallower units; however, they are incapable of detecting the upper ca. 10 m sedimentary units. Accordingly, a shallow seismic survey is recommended to fill the gaps from the other surveys.

The intermediate offshore profile shooting, perpendicular and parallel to the coastline, has been performed on 20–30 km remote distances from the Bushehr Peninsula (Atomstroyexport, 1999), which covers the depths up to 300 m. Atomstroyexport (1999) suggest no fault presence in the seismic profiles. However, our interpretations based on these seismic data show fauling evidence (Figure 13) and imply an event horizon at depths lower than 5–10 m below the seafloor. Additionally, our estimates based on the data from (Hosseinyar et al., 2021) (Table 2) suggest a sedimentation rate of 1.045±0.46 mm/yr. The depth of the event horizon and the rate of sedimentation, boost the likelihood of moderate- to large-sized earthquakes during the Holocene.

Table 2: Radiocarbon (14C) ages of the samples obtained from Bu-A borehole core in the Bushehr Peninsula (Hosseinyar et al., 2021).

Core Depth (m)	Age (ka BP)	Sample type
0.59	2.840	Benthic shell
1.44	3.320	Benthic shell
4.04	4.025	Benthic shell
5.93	4.695	Benthic shell
6.74	5.610	Benthic shell
9.56	7.425	Benthic shell
10.12	7.115	Benthic shell
11.67	7.105	Benthic shell
14.77	15.600	

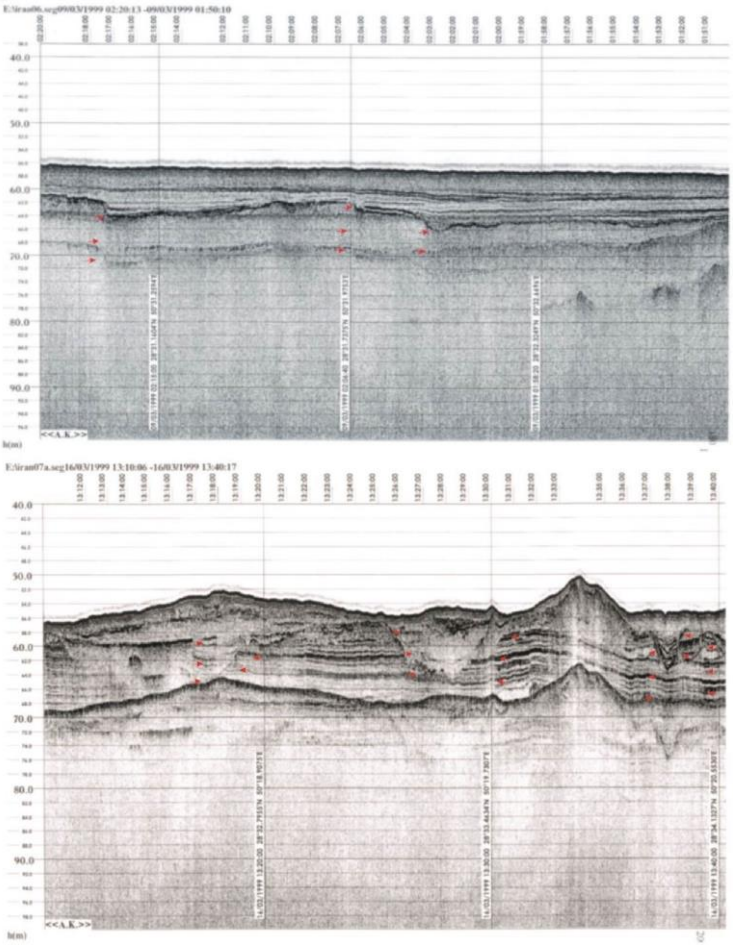

Figure 13: Examples of the intermediate, offshore seismic profiles (southwest of the Bushehr Peninsula), indicating event horizon at depths of 50–60 m with a ca. 5–10 m young sedimentary cover (up). Red arrows denote the faults.

9.2 Furg earthquake

The Mw 6.4 Furg earthquake of 6 November 1990 is a unique earthquake within the Zagros where the fault ruptured to the surface (e.g., Talebian and Jackson, 2004; R. T. Walker et al., 2005). The Covid-19 crisis and the prolonged lockdowns imposed immense limitations and consequently interruptions in the foreseen schedule, which was one of the biggest challenges and delayed the entire research and study process. The field studies have been aborted; accordingly, trenching, sampling, and further data have become inaccessible, which largely affected my plans to accomplish the investigations along the epicentral area of the Furg earthquake.

I had to omit a chapter of the thesis for which I had previously acquired data, such as a full dataset of two generations of the precisely scanned negatives of aerial photos of the Furg study area, and performed the first field investigations for a paleoseismological site selection. I carried out a Structure from Motion (SfM) algorithm, implemented in the MicMac free opensource photogrammetric library (Rupnik et al., 2017), to generate multi-temporal, ultra-highresolution Digital Surface Models (DSMs) from the aerial photos datasets (Figure 14). An impending plan for paleoseismological excavations would fulfill the data to accomplish the impaired study within the Furg study area.

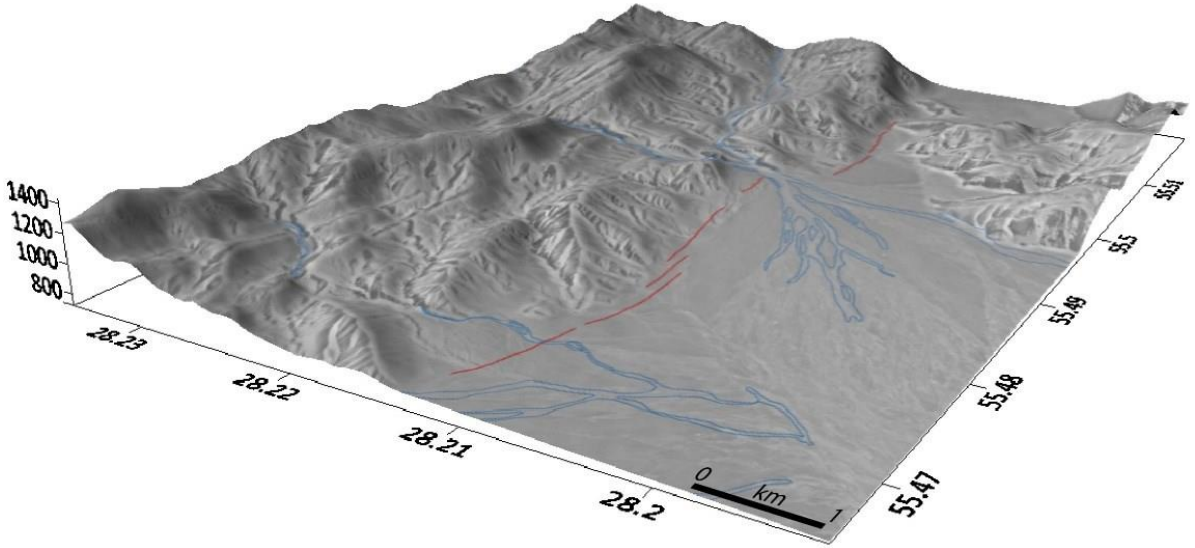

Figure 14:Orthomosaic aerial photos draped on a 1-m resolution digital surface model (DSM) derived from historical aerial photos of 1967 (scale 1:20,000) using MicMac open-source software. Red lines illustrate the surface rupture of the Mw 6.4 Furg earthquake (6 November 1990).

9.3 Khonj earthquake

On 6 January 2017, an Mw 4.9 earthquake occurred ca. 40 km northeast of the city of Khonj (Figure 15a), in the Simply Folded Belt (SFB) of the Zagros, southwestern Iran. Using the JAXA ALOS-2 PALSAR as well as the Copernicus Sentinel-1 SAR images, I applied two-pass Interferometric Synthetic Aperture Radar (InSAR) to acquire the corresponding surface deformation of the Khonj earthquake. The fault plane solutions (e.g., IRSC) confirm the thrust mechanism for the earthquake that has a shallow depth of 5 km (IRSC) resulting in a subtle, permanent surface deformation (Figure 15c, e) visible through InSAR displacement maps (Figure 15b, d, and f). Concentric fringes on the interferograms in both ascending and descending geometries indicate the rupture has not reached the surface; nonetheless, indicate shallow seismic deformation within the Zagros Rupture Band (ZRB; see details in Chapter 8, Figure 11). The Khonj earthquake is one of the smallest events with a discernible InSAR deformation field of ca. 5-10 cm in the satellite line-of-sight (LOS). The epicenter of the earthquake is located in a plain between the northwestern and southeastern hinges of the Qul Qul and Nahreh anticlines. This shallow event is aligned with a zone in which the only documented surface ruptures in the Zagros-i.e., the Furg (e.g., R. T. Walker et al., 2005) and Qir-Karzin (e.g.,

Dewey and Grantz, 1973) earthquakes are located. The source modeling from the InSAR data quantifies an NW-SE-striking fault either dipping to the northeast or the southwest. To validate the associated source, filed studies of the epicentral area as well as the structural configuration of the area are necessary. However, similar to the paleoseismological investigations in the Furg area, the field survey in the Khonj area was not possible due to the Covid-19 pandemic restrictions. The Khonj event is yet an interesting case to be studied combined with field observations.

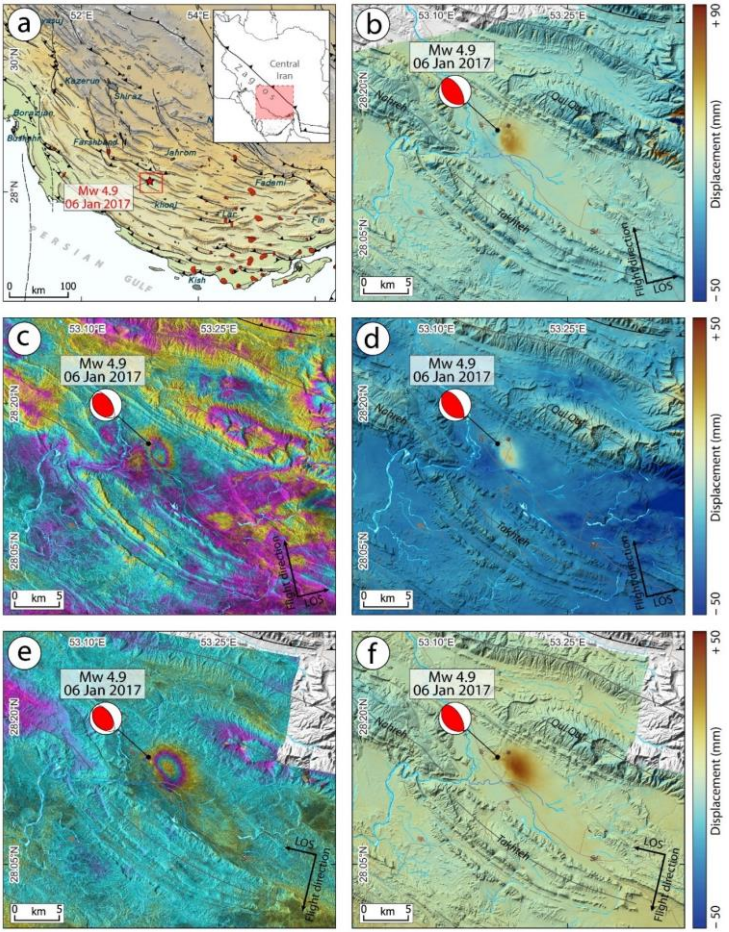

Figure 15: a) Tectonic configuration of the Fars Arc and the Simply Folded Belt (SFB) in the central Zagros. Red star denotes the epicenter of the Mw 4.9 Khonj earthquake (6 January 2017) located in the Zagros Rupture Band (ZRB). b, d, and f) Line-of-sight (LOS) displacement maps of the Khonj event derived from the descending ALOS-2, and the ascending (c) and descending (e) Sentinel-1 interferograms.

References

Agard, P., Omrani, J., Jolivet, L., Mouthereau, F., 2005. Convergence history across Zagros (Iran): constraints from collisional and earlier deformation. Int J Earth Sci (Geol Rundsch) 94, 401–419. https://doi.org/10.1007/s00531-005-0481-4

Alavi, M., 2007. Structures of the Zagros fold-thrust belt in Iran. American Journal of Science 307, 1064–1095. https://doi.org/10.2475/09.2007.02

Alavi, M., 1994. Tectonics of the Zagros orogenic belt of Iran: new data and interpretations. Tectonophysics 229, 211–238.

Allen, M.B., Saville, C., Blanc, E.J.-P., Talebian, M., Nissen, E., 2013. Orogenic plateau growth: Expansion of the Turkish-Iranian Plateau across the Zagros fold-and-thrust belt. Tectonics 32, 171–190. https://doi.org/10.1002/tect.20025

Ambraseys, N.N., Melville, C.P., 1982. A History of Persian Earthquakes. Cambridge University Press, London.

Atomstroyexport, 1999. Supplementary Site Investigations for Evaluation of Design Basis Parameters of the Unit (Unpublished report No. 95.BU.1

Bahroudi, A., Koyi, H.A., 2004. Tectono-sedimentary framework of the Gachsaran Formation in the Zagros foreland basin. Marine and Petroleum Geology 21, 1295–1310. https://doi.org/10.1016/j.marpetgeo.2004.09.001

Bahroudi, A., Koyi, H.A., 2003. Effect of spatial distribution of Hormuz salt on deformation style in the Zagros fold and thrust belt: an analogue modelling approach. Journal of the Geological Society 160, 719–733. https://doi.org/10.1144/0016-764902-135

Bahroudi, A., Talbot, C.J., 2003. The configuration of the basement beneath the Zagros basin. Journal of Petroleum Geology 26, 257–282. https://doi.org/10.1111/j.1747-5457.2003.tb00030.x

Baker, C., Jackson, J., Priestley, K., 1993. Earthquakes on the Kazerun Line in the Zagros Mountains of Iran: strike-slip faulting within a fold-and-thrust belt. Geophysical Journal International 115, 41–61. https://doi.org/10.1111/j.1365-246X.1993.tb05587.x

Barnhart, W.D., Brengman, C.M.J., Li, S., Peterson, K.E., 2018. Ramp-flat basement structures of the Zagros Mountains inferred from co-seismic slip and afterslip of the 2017 Mw7.3 Darbandikhan,

Iran/Iraq earthquake. Earth and Planetary Science Letters 496, 96–107. https://doi.org/10.1016/j.epsl.2018.05.036

Barnhart, W.D., Lohman, R.B., 2013. Phantom earthquakes and triggered aseismic creep: Vertical partitioning of strain during earthquake sequences in Iran. Geophysical Research Letters 40, 819–823. https://doi.org/10.1002/grl.50201

Barnhart, W.D., Lohman, R.B., Mellors, R.J., 2013. Active accommodation of plate convergence in Southern Iran: Earthquake locations, triggered aseismic slip, and regional strain rates: southern Iran active deformation. Journal of Geophysical Research: Solid Earth 118, 5699–5711. https://doi.org/10.1002/jgrb.50380

Berardino, P., Fornaro, G., Lanari, R., Sansosti, E., 2002. A new algorithm for surface deformation monitoring based on small baseline differential SAR interferograms. IEEE Trans. Geosci. Remote Sensing 40, 2375–2383. https://doi.org/10.1109/TGRS.2002.803792

Berberian, F., Muir, I.D., Pankhurst, R.J., Berberian, M., 1982. Late Cretaceous and early Miocene Andean-type plutonic activity in northern Makran and Central Iran. Journal of the Geological Society

139, 605–614. https://doi.org/10.1144/gsjgs.139.5.0605

Berberian, M., 2014. Earthquakes and coseismic surface faulting on the Iranian Plateau: a historical, social and physical approach, 1st ed, Developments in Earth Surface Processes. Elsevier Science, Amsterdam.

Berberian, M., 1995. Master "blind" thrust faults hidden under the Zagros folds: active basement tectonics and surface morphotectonics. Tectonophysics 241, 193–224. https://doi.org/10.1016/0040-1951(94)00185-C

Berberian, M., 1983. Continental Deformation in the Iranian Plateau (Contribution to the Seismotectonics of Iran, Part IV). Geological Survey of Iran.

Berberian, M., King, G.C.P., 1981. Towards a paleogeography and tectonic evolution of Iran. Can. J. Earth Sci. 18, 210–265. https://doi.org/10.1139/e81-019

Berberian, M., Yeats, R.S., 2001. Contribution of archaeological data to studies of earthquake history in the Iranian Plateau. Journal of Structural Geology 23, 563–584. https://doi.org/10.1016/S0191-8141(00)00115-2

Berberian, M., Yeats, R.S., 1999. Patterns of Historical Earthquake Rupture in the Iranian Plateau. Bulletin of the Seismological Society of America 89, 120–139.

Blanc, E.J.-P., Allen, M.B., Inger, S., Hassani, H., 2003. Structural styles in the Zagros Simple Folded Zone, Iran. Journal of the Geological Society 160, 401–412. https://doi.org/10.1144/0016-764902-110

Bürgmann, R., Rosen, P.A., Fielding, E.J., 2000. Synthetic Aperture Radar Interferometry to Measure Earth's Surface Topography and Its Deformation. Annu. Rev. Earth Planet. Sci. 28, 169–209. https://doi.org/10.1146/annurev.earth.28.1.169

Casu, F., Manzo, M., Lanari, R., 2006. A quantitative assessment of the SBAS algorithm performance for surface deformation retrieval from DInSAR data. Remote Sensing of Environment 102, 195–210. https://doi.org/10.1016/j.rse.2006.01.023

Chen, K., Xu, W., Mai, P.M., Gao, H., Zhang, L., Ding, X., 2018. The 2017 Mw 7.3 Sarpol Zahāb Earthquake, Iran: A compact blind shallow-dipping thrust event in the mountain front fault basement. Tectonophysics 747–748, 108–114. https://doi.org/10.1016/j.tecto.2018.09.015

Colman-Sadd, S.P., 1978. Fold Development in Zagros Simply Folded Belt, Southwest Iran. Bulletin 62. https://doi.org/10.1306/C1EA4F81-16C9-11D7-8645000102C1865D

Copley, A., Karasozen, E., Oveisi, B., Elliott, J.R., Samsonov, S., Nissen, E., 2015. Seismogenic faulting of the sedimentary sequence and laterally variable material properties in the Zagros Mountains (Iran) revealed by the August 2014 Murmuri (E. Dehloran) earthquake sequence. Geophys. J. Int. 203, 1436–1459. https://doi.org/10.1093/gji/ggv365

Costantini, M., 1998. A novel phase unwrapping method based on network programming. IEEE Trans. Geosci. Remote Sensing 36, 813–821. https://doi.org/10.1109/36.673674

de Lamotte, D.F., Leturmy, P., 2013. Structural map of the Arabian plate and surrounding areas. Delvaux, D., Sperner, B., 2003. New aspects of tectonic stress inversion with reference to the TENSOR program. Geological Society, London, Special Publications 212, 75–100. https://doi.org/10.1144/GSL.SP.2003.212.01.06

Dewey, J.W., Grantz, A., 1973. The Ghir earthquake of April 10, 1972 in the Zagros Mountains of southern Iran: seismotectonic aspects and some

results of a field reconnaissance.Bulletin of the Seismological Society of America 63, 2071–2090. https://doi.org/10.1785/BSSA0636-12071

Ding, K., He, P., Wen, Y., Chen, Y., Wang, D., Li, S., Wang, Q., 2018. The 2017 Mw 7.3 Ezgeleh, Iran earthquake determined from InSAR measurements and teleseismic waveforms. Geophysical Journal International 215, 1728–1738. https://doi.org/10.1093/gji/ggy371

Elliott, J.R., Bergman, E.A., Copley, A.C., Ghods, A.R., Nissen, E.K., Oveisi, B., Tatar, M., Walters, R.J., Yamini-Fard, F., 2015. The 2013 Mw 6.2 Khaki-Shonbe (Iran) Earthquake: Insights into seismic and aseismic shortening of the Zagros sedimentary cover. Earth and Space Science 2, 435–471. https://doi.org/10.1002/2015EA000098

Falcon, N.L., 1974. Southern Iran: Zagros Mountains. Geological Society, London, Special Publications 4, 199–211. https://doi.org/10.1144/GSL.SP.2005.004.01.11

Falcon, N.L., 1969. Problems of the relationship between surface structure and deep displacements illustrated by the Zagros Range. Geological Society, London, Special Publications 3, 9–21. https://doi.org/10.1144/GSL.SP.1969.003.01.02

Fathian, A., Atzori, S., Nazari, H., Reicherter, K., Salvi, S., Svigkas, N., Tatar, M., Tolomei, C., Yaminifard, F., 2021. Complex co- and postseismic faulting of the 2017–2018 seismic sequence in western Iran revealed by InSAR and seismic data. Remote Sensing of Environment 253, 112224. https://doi.org/10.1016/j.rse.2020.112224

Fathian, A., Atzori, S., Nazari, H., Reicherter, K., Salvi, S., Tolomei, C., Fard, F.Y., 2019. Modeling the sources of the Azgeleh (12 November 2017) and Tazehabad (25 August 2018) earthquakes, Western Iran. Presented at the European Geophysical Union (EGU) General Assembly 2019, Vienna, Austria, p. 1.

Fathian, A., Shokri, M.A., Nazari, H., Ghorashi, M., 2016. Morphotectonic Map of Bushehr Region.

Feng, W., Samsonov, S., Almeida, R., Yassaghi, A., Li, J., Qiu, Q., Li, P., Zheng, W., 2018. Geodetic Constraints of the 2017 Mw 7.3 Sarpol Zahab, Iran Earthquake, and Its Implications on the Structure and Mechanics of the Northwest Zagros Thrust-Fold Belt. Geophys. Res. Lett. 45, 6853–6861. https://doi.org/10.1029/2018GL078577

Ferretti, A., Prati, C., Rocca, F., 2001. Permanent scatterers in SAR interferometry. IEEE Trans. Geosci. Remote Sensing 39, 8–20. https://doi.org/10.1109/36.898661

Goldstein, R.M., Werner, C.L., 1998. Radar interferogram filtering for geophysical applications. Geophys. Res. Lett. 25, 4035–4038. https://doi.org/10.1029/1998GL900033

Gombert, B., Duputel, Z., Shabani, E., Rivera, L., Jolivet, R., Hollingsworth, J., 2019. Impulsive Source of the 2017 Mw =7.3 Ezgeleh, Iran, Earthquake. Geophys. Res. Lett. 2018GL081794. https://doi.org/10.1029/2018GL081794

Hatzfeld, D., Tatar, M., Priestley, K., Ghafory-Ashtiany, M., 2003. Seismological constraints on the crustal structure beneath the Zagros Mountain belt (Iran). Geophysical Journal International 155, 403–410. https://doi.org/10.1046/j.1365-246X.2003.02045.x

Haynes, S.J., McQuillan, H., 1974. Evolution of the Zagros Suture Zone, Southern Iran. Geological Society of America Bulletin 85, 739–744.

Hessami, K., Jamali, F., Tabasi, H., 2003. Major Active Faults of Iran.

Hessami, K., Koyi, H.A., Talbot, C.J., 2001. The significance of strike-slip faulting in the basement

of the Zagros fold and thrust belt. Journal of Petroleum Geology 24, 5–28. ttps://doi.org/10.1111/j.1747-5457.2001.tb00659.x

Hessami, K., Nilforoushan, F., Talbot, C.J., 2006. Active deformation within the Zagros Mountains deduced from GPS measurements. Journal of the Geological Society 163, 143–148. https://doi.org/10.1144/0016-764905-031

Honda, R., Aoi, S., 2009. Array Back-Projection Imaging of the 2007 Niigataken Chuetsu-oki Earthquake Striking the World's Largest Nuclear Power Plant. Bulletin of the Seismological Society of America 99, 141–147. https://doi.org/10.1785/0120080062

Hooper, A., 2008. A multi-temporal InSAR method incorporating both persistent scatterer and small baseline approaches. Geophys. Res. Lett. 35, L16302. https://doi.org/10.1029/2008GL034654

Hooper, A., Bekaert, D., Spaans, K., Arıkan, M., 2012. Recent advances in SAR interferometry time series analysis for measuring crustal deformation. Tectonophysics 514–517, 1– 13. https://doi.org/10.1016/j.tecto.2011.10.013

Hosseinyar, G., Behbahani, R., Moussavi-Harami, R., Lak, R., Kuijpers, A., 2021. Holocene sealevel changes of the Persian Gulf. Quaternary

International 571, 26–45. https://doi.org/10.1016/j.quaint.2020.11.051

Ishii, M., Shearer, P.M., Houston, H., Vidale, J.E., 2007. Teleseismic P wave imaging of the 26 December 2004 Sumatra-Andaman and 28 March 2005 Sumatra earthquake ruptures using the Hi-net array. Journal of Geophysical Research 112, B11307. https://doi.org/10.1029/2006JB004700

Ishii, M., Shearer, P.M., Houston, H., Vidale, J.E., 2005. Extent, duration and speed of the 2004 Sumatra–Andaman earthquake imaged by the Hi-Net array. Nature 435, 933–936. https://doi.org/10.1038/nature03675

Jackson, J., 1992. Partitioning of strike-slip and convergent motion between Eurasia and Arabia in eastern Turkey and the Caucasus. Journal of Geophysical Research 97, 12471. https://doi.org/10.1029/92JB00944

Jackson, J., Fitch, T., 1981. Basement faulting and the focal depths of he larger earthquakes in the Zagros mountains (Iran). Geophysical Journal of the Royal Astronomical Society 64, 561–586. https://doi.org/10.1111/j.1365-246X.1981.tb02685.x

Jackson, J., McKenzie, D., 1984. Active tectonics of the Alpine--Himalayan Belt between western Turkey and Pakistan. Geophysical Journal International 77, 185–264. https://doi.org/10.1111/j.1365-246X.1984.tb01931.x

Jahani, S., Callot, J.-P., Letouzey, J., Frizon de Lamotte, D., 2009. The eastern termination of the Zagros Fold-and-Thrust Belt, Iran: Structures, evolution, and relationships betwee salt plugs, folding, and faulting. Tectonics 28, n/a-n/a. https://doi.org/10.1029/2008TC002418

Karasözen, E., Nissen, E., Bergman, E.A., Ghods, A., 2019. Seismotectonics of the Zagros (Iran) From Orogen-Wide, Calibrated Earthquake Relocations. Journal of Geophysical Research: Solid Earth 2019JB017336. https://doi.org/10.1029/2019JB017336

Karimzadeh, S., Matsuoka, M., Miyajima, M., Adriano, B., Fallahi, A., Karashi, J., 2018. Sequential SAR Coherence Method for the Monitoring of Buildings in Sarpole-Zahab, Iran. Remote Sensing 10, 1255. https://doi.org/10.3390/rs10081255

Kennett, B.L.N., Engdahl, E.R., 1991. Traveltimes for global earthquake location and phase identification. Geophysical Journal International

105, 429–465. ttps://doi.org/10.1111/j.1365-246X.1991.tb06724.x

Kent, P.E., 1979. The emergent Hormuz salt plugs of southern Iran. Journal of Petroleum Geology 2, 117–144. https://doi.org/10.1111/j.1747-5457.1979.tb00698.x

Khorrami, F., Vernant, P., Masson, F., Nilfouroushan, F., Mousavi, Z., Nankali, H., Saadat, S.A., Walpersdorf, A., Hosseini, S., Tavakoli, P., Aghamohammadi, A., Alijanzade, M., 2019. An up-to-date crustal deformation map of Iran using integrated campaign-mode and permanent GPS velocities. Geophysical Journal International 217, 832–843. https://doi.org/10.1093/gji/ggz045

Kiser, E., Ishii, M., 2017. Back-Projection Imaging of Earthquakes. Annual Review of Earth and Planetary Sciences 45, 271–299. https://doi.org/10.1146/annurev-earth-063016-015801

Kiser, E., Ishii, M., Langmuir, C.H., Shearer, P.M., Hirose, H., 2011. Insights into the mechanism of intermediate-depth earthquakes from source properties as imaged by back projection of multiple seismic phases. J. Geophys. Res. 116, B06310. https://doi.org/10.1029/2010JB007831

Kissling, E., 1988. Geotomography with local earthquake data. Rev. Geophys. 26, 659–698. https://doi.org/10.1029/RG026i004p00659

Koyi, H.A., Ghasemi, A., Hessami, K., Dietl, C., 2008. The mechanical relationship between strikeslip faults and salt diapirs in the Zagros fold–thrust belt. Journal of the Geological Society 165, 1031–1044. https://doi.org/10.1144/0016-76492007-142

Kuang, J., Ge, L., Metternicht, G.I., Ng, A.H.-M., Wang, H., Zare, M., Kamranzad, F., 2019. Coseismic deformation and source model of the 12 November 2017 Mw 7.3 Kermanshah Earthquake (Iran–Iraq border) investigated through DInSAR measurements. International Journal of Remote Sensing 40, 532–554. https://doi.org/10.1080/01431161.2018.1514542

Lienert, B.R., Havskov, J., 1995. A Computer Program for Locating Earthquakes Both Locally and Globally. Seismological Research Letters 66, 26–36. https://doi.org/10.1785/gssrl.66.5.26

Lv, X., Amelung, F., Shao, Y., Ye, S., Liu, M., Xie, C., 2020. Rheology of the Zagros Lithosphere from Post-Seismic Deformation of the 2017 Mw7.3 Kermanshah, Iraq, Earthquake. Remote Sensing 12, 2032. https://doi.org/10.3390/rs12122032

Maggi, A., Jackson, J.A., Priestley, K., Baker, C., 2000. A re-assessment of focal depth distributions in southern Iran, the Tien Shan and northern India: do earthquakes really occur in the continental mantle? Geophysical Journal International 143, 629–661 . https://doi.org/10.1046/j.1365-246X.2000.00254.x

Masson, F., Chéry, J., Hatzfeld, D., Martinod, J., Vernant, P., Tavakoli, F., Ghafory-Ashtiani, M., 2005. Seismic versus aseismic deformation in Iran inferred from earthquakes and geodetic data: Seismic versus aseismic deformation in Iran. Geophysical Journal International 160, 217–226. https://doi.org/10.1111/j.1365-246X.2004.02465.x

Massonnet, D., Rossi, M., Carmona, C., Adragna, F., Peltzer, G., Feigl, K., Rabaute, T., 1993. The displacement field of the Landers earthquake mapped by radar interferometry. Nature 364, 138–142. https://doi.org/10.1038/364138a0

McKenzie, D., 1972. Active Tectonics of the Mediterranean Region. Geophysical Journal International 30, 109–185. https://doi.org/10.1111/j.1365-246X.1972.tb02351.x

McQuarrie, N., 2004. Crustal scale geometry of the Zagros fold–thrust belt, Iran. Journal of Structural

Geology 26, 519–535. https://doi.org/10.1016/j.jsg.2003.08.009

Miyajima, M., Fallahi, A., Ikemoto, T., Samaei, M., Karimzadeh, S., Setiawan, H., Talebi, F., Karashi, J., 2018. Site Investigation of the Sarpole-Zahab Earthquake, Mw 7.3 in SW Iran of November 12, 2017

Molinaro, M., Leturmy, P., Guezou, J.-C., Frizon de Lamotte, D., Eshraghi, S.A., 2005. The structure and kinematics of the southeastern Zagros fold-thrust belt, Iran: From thinskinned to thick-skinned tectonics. Tectonics 24, n/a-n/a. https://doi.org/10.1029/2004TC001633

Motagh, M., Bahroudi, A., Haghighi, M.H., Samsonov, S., Fielding, E., Wetzel, H.-U., 2015. The 18 August 2014 Mw 6.2 Mormori, Iran, Earthquake: A Thin-Skinned Faulting in the Zagros Mountain Inferred from InSAR Measurements. Seismological Research Letters 86, 775– 782. https://doi.org/10.1785/0220140222

Mouthereau, F., Lacombe, O., Vergés, J., 2012. Building the Zagros collisional orogen: Timing, strain distribution and the dynamics of Arabia/Eurasia plate convergence. Tectonophysics 532–535, 27–60. https://doi.org/10.1016/j.tecto.2012.01.022

Nazari, H., Talebian, M., Ghorashi, M., 2013. Seismotectonic Map of NW Iran.

Ni, J., Barazangi, M., 1986. Seismotectonics of the Zagros continental collision zone and a comparison with the Himalayas. Journal of Geophysical Research 91, 8205. https://doi.org/10.1029/JB091iB08p08205

Nilforoushan, F., Masson, F., Vernant, P., Vigny, C., Martinod, J., Abbassi, M., Nankali, H., Hatzfeld, D., Bayer, R., Tavakoli, F., Ashtiani, A., Doerflinger, E., Daignières, M., Collard, P., Chéry, J., 2003. GPS network monitors the Arabia-Eurasia collision deformation in Iran. Journal of Geodesy 77, 411–422. https://doi.org/10.1007/s00190-003-0326-5

Nissen, E., Ghods, A., Karasözen, E., Elliott, J.R., Barnhart, W.D., Bergman, E.A., Hayes, G.P., Jamal- Reyhani, M., Nemati, M., Tan, F., Abdulnaby, W., Benz, H.M., Shahvar, M.P., Talebian, M., Chen, L., 2019. The 12 November 2017 Mw 7.3 Ezgeleh-Sarpolzahab (Iran) Earthquake and Active Tectonics of the Lurestan Arc. J. Geophys. Res. Solid Earth 124, 2124–2152. https://doi.org/10.1029/2018JB016221

Nissen, E., Tatar, M., Jackson, J.A., Allen, M.B., 2011. New views on earthquake faulting in the Zagros

fold-and-thrust belt of Iran: Earthquake faulting in the Zagros. Geophysical Journal International 186, 928–944. https://doi.org/10.1111/j.1365-246X.2011.05119.x

Nocquet, J.-M., 2012. Present-day kinematics of the Mediterranean: A comprehensive overview of GPS results. Tectonophysics 579, 220–242. https://doi.org/10.1016/j.tecto.2012.03.037

O'Brien, C.A.E., 1957. Salt diapirism in south Persia 19, 357–376.

Olen, S., Bookhagen, B., 2018. Mapping Damage-Affected Areas after Natural Hazard Events Using Sentinel-1 Coherence Time Series. Remote Sensing 10, 1272. https://doi.org/10.3390/rs10081272

Oveisi, B., Lavé, J., van der Beek, P., 2007. Rates and Processes of Active Folding Evidenced by Pleistocene Terraces at the Central Zagros Front (Iran), in: Lacombe, O., Roure, F., Lavé, J., Vergés, J. (Eds.), Thrust Belts and Foreland Basins. Springer Berlin Heidelberg, Berlin, Heidelberg, pp. 267–287. https://doi.org/10.1007/978-3-540-69426-7_14

Pulido, N., Aoi, S., Fujiwara, H., 2008. Rupture process of the 2007 Notohanto earthquake by using an isochrones back-projection method and K-

NET/KiK-net data. Earth, Planets and Space 60, 1035–1040. https://doi.org/10.1186/BF03352865

Rhodes, E.J., 2011. Optically Stimulated Luminescence Dating of Sediments over the Past 200,000 Years. Annual Review of Earth and Planetary Sciences 39, 461–488. https://doi.org/10.1146/annurev-earth-040610-133425

Roustaei, M., Nissen, E., Abbassi, M., Gholamzadeh, A., Ghorashi, M., Tatar, M., Yamini-Fard, F., Bergman, E., Jackson, J., Parsons, B., 2010. The 2006 March 25 Fin earthquakes (Iran)- insights into the vertical extents of faulting in the Zagros Simply Folded Belt. Geophysical Journal International. https://doi.org/10.1111/j.1365-246X.2010.04601.x

Rupnik, E., Daakir, M., Pierrot Deseilligny, M., 2017. MicMac – a free, open-source solution for photogrammetry. Open geospatial data, softw. stand. 2, 14. https://doi.org/10.1186/s40965-017-0027-2

Sherkati, S., Letouzey, J., 2004. Variation of structural style and basin evolution in the central Zagros (Izeh zone and Dezful Embayment), Iran. Marine and Petroleum Geology 21, 535–554. https://doi.org/10.1016/j.marpetgeo.2004.01.007

Sherkati, S., Letouzey, J., Frizon de Lamotte, D., 2006. Central Zagros fold-thrust belt (Iran): New insights from seismic data, field observation, and sandbox modeling: Central Zagros Fold-Thrust Belt. Tectonics 25, n/a-n/a. https://doi.org/10.1029/2004TC001766

Shirakova, E.I., 1967. General features in the orientation of principal stresses in earthquake foci in the Mediterranean–Asian seismic belt. Earth Phys. 1, 22–36.

Stöcklin, J., 1974. Possible Ancient Continental Margins in Iran, in: Burk, C.A., Drake, C.L. (Eds.), The Geology of Continental Margins. Springer Berlin Heidelberg, Berlin, Heidelberg, pp. 873–887. https://doi.org/10.1007/978-3-662-01141-6_64

Stöcklin, J., 1968. Structural history and tectonics of Iran: A review. American Association of Petroleum Geologists Bulletin 52, 1229–1258.

Talbot, C.J., Alavi, M., 1996. The past of a future syntaxis across the Zagros. Geological Society, London, Special Publications 100, 89–109. https://doi.org/10.1144/GSL.SP.1996.100.01.08

Talebian, M., Jackson, J., 2004. A reappraisal of earthquake focal mechanisms and active shortening in the Zagros mountains of Iran.

Geophysical Journal International 156, 506–526. https://doi.org/10.1111/j.1365-246X.2004.02092.x

Tavani, S., Parente, M., Puzone, F., Corradetti, A., Gharabeigli, G., Valinejad, M., Morsalnejad, D., Mazzoli, S., 2018. The seismogenic fault system of the 2017 Mw 7.3 Iran–Iraq earthquake: constraints from surface and subsurface data, cross-section balancing, and restoration. Solid Earth 9, 821–831. https://doi.org/10.5194/se-9-821-2018

Tolomei, C., Svigkas, N., Baneh, A.F., Atzori, S., Pezzo, G., 2018. Surface Deformation and Source Modeling for the Mw 7.3 Iran Earthquake (November 12, 2017) Exploiting Sentinel-1 and ALOS-2 Insar Data, in: IGARSS 2018 - 2018 IEEE International Geoscience and Remote Sensing Symposium. Presented at the IGARSS 2018 - 2018 IEEE International Geoscience and Remote Sensing Symposium, IEEE, Valencia, pp. 3063–3066. https://doi.org/10.1109/IGARSS.2018.8518173

Vajedian, S., Motagh, M., Mousavi, Z., Motaghi, K., Fielding, Eric., Akbari, B., Wetzel, H.-U., Darabi, A., 2018. Coseismic Deformation Field of the Mw 7.3 12 November 2017 Sarpol-e Zahab (Iran) Earthquake: A Decoupling Horizon in the Northern Zagros Mountains Inferred from InSAR

Observations. Remote Sensing 10, 1589. https://doi.org/10.3390/rs10101589

Vernant, Ph., Nilforoushan, F., Hatzfeld, D., Abbassi, M.R., Vigny, C., Masson, F., Nankali, H., Martinod, J., Ashtiani, A., Bayer, R., Tavakoli, F., Chéry, J., 2004. Present-day crustal deformation and plate kinematics in the Middle East constrained by GPS measurements in Iran and northern Oman. Geophysical Journal International 157, 381–398. https://doi.org/10.1111/j.1365-246X.2004.02222.x

Waldhauser, F., 2000. A Double-Difference Earthquake Location Algorithm: Method and Application to the Northern Hayward Fault, California. Bulletin of the Seismological Society of America 90, 1353–1368. https://doi.org/10.1785/0120000006

Walker, K.T., Ishii, M., Shearer, P.M., 2005. Rupture details of the 28 March 2005 Sumatra Mw 8.6 earthquake imaged with teleseismic P waves. Geophysical Research Letters 32, L24303. https://doi.org/10.1029/2005GL024395

Walker, K.T., Shearer, P.M., 2009. Illuminating the near-sonic rupture velocities of the intracontinental Kokoxili Mw 7.8 and Denali fault Mw 7.9 strike-slip earthquakes with global P wave back projection imaging. Journal of Geophysical

Research 114, B02304. https://doi.org/10.1029/2008JB005738

Walker, M.J.C., 2005. Quaternary dating methods. J. Wiley, Chichester, West Sussex, England.

Walker, R.T., Andalibi, M.J., Gheitanchi, M.R., Jackson, J.A., Karegar, S., Priestley, K., 2005. Seismological and field observations from the 1990 November 6 Furg (Hormozgan) earthquake: a rare case of surface rupture in the Zagros mountains of Iran. Geophysical Journal International 163, 567–579. https://doi.org/10.1111/j.1365- 246X.2005.02731.x

Walpersdorf, A., Hatzfeld, D., Nankali, H., Tavakoli, F., Nilforoushan, F., Tatar, M., Vernant, P., Chéry, J., Masson, F., 2006. Difference in the GPS deformation pattern of North and Central Zagros (Iran). Geophysical Journal International 167, 1077–1088. https://doi.org/10.1111/j.1365-246X.2006.03147.x

Wang, K., Bürgmann, R., 2020. Probing Fault Frictional Properties During Afterslip Updip and Downdip of the 2017 Mw 7.3 Sarpol-e Zahab Earthquake With Space Geodesy. J. Geophys. Res. Solid Earth 125. https://doi.org/10.1029/2020JB020319

Wang, K., Bürgmann, R., 2018. Probing fault frictional properties during afterslip up- and down-dip of the

2017 Mw 7.3 Iran-Iraq earthquake, in: 2018 SCEC Annual Meeting. Presented at the 2018 SCEC Annual Meeting.

Wang, Z., Zhang, R., Wang, X., Liu, G., 2018. Retrieving Three-Dimensional Co-Seismic Deformation of the 2017 Mw7.3 Iraq Earthquake by Multi-Sensor SAR Images. Remote Sensing 10, 857. https://doi.org/10.3390/rs10060857

Washaya, P., Balz, T., 2018. SAR COHERENCE CHANGE DETECTION OF URBAN AREAS AFFECTED BY DISASTERS USING SENTINEL-1 IMAGERY. Int. Arch. Photogramm. Remote Sens. Spatial Inf. Sci. XLII–3, 1857–1861. https://doi.org/10.5194/isprsarchives-XLII-3-1857-2018

Yang, Y., Hu, J., Yassaghi, A., Tsai, M., Zare, M., Chen, Q., Wang, Z., Rajabi, A.M., Kamranzad, F., 2018. Midcrustal Thrusting and Vertical Deformation Partitioning Constraint by 2017 Mw 7.3 Sarpol Zahab Earthquake in Zagros Mountain Belt, Iran. Seismological Research Letters 89, 2204–2213. https://doi.org/10.1785/0220180022

Zebker, H.A., Rosen, P.A., Goldstein, R.M., Gabriel, A., Werner, C.L., 1994. On the derivation of coseismic displacement fields using differential radar interferometry: The Landers earthquake. J.

Geophys. Res. 99, 19617–19634. https://doi.org/10.1029/94JB01179

Zebker, H.A., Villasenor, J., 1992. Decorrelation in interferometric radar echoes. IEEE Trans. Geosci. Remote Sensing 30, 950–959. https://doi.org/10.1109/36.175330